Global and Planetary Change 162 (2018) 53–68

Contents lists available at ScienceDirect

Global and Planetary Change

journal homepage: www.elsevier.com/locate/gloplacha

The Early Toarcian oceanic anoxic event: Paleoenvironmental and paleoclimatic change across the Alpine Tethys (Switzerland)

Alicia Fantasia[a,*], Karl B. Föllmi[a], Thierry Adatte[a], Jorge E. Spangenberg[b], Jean-Carlos Montero-Serrano[c,d]

[a] Institute of Earth Sciences (ISTE), University of Lausanne, 1015 Lausanne, Switzerland
[b] Institute of Earth Surface Dynamics (IDYST), University of Lausanne, 1015 Lausanne, Switzerland
[c] Marine Sciences Institute (ISMER), University of Quebec in Rimouski, Rimouski, Quebec, G5L 3A1, Canada
[d] GEOTOP Research Center, C.P. 8888, Montreal, QC H3C 3P8, Canada

ARTICLE INFO

Keywords:
Toarcian OAE
Proximal-distal transect
Mineralogy
Geochemistry
Phosphorus
Climate change

ABSTRACT

Paleoenvironmental and paleoclimatic change associated with the Toarcian oceanic anoxic event (T-OAE) was evaluated in five successions located in Switzerland. They represent different paleogeographic settings across the Alpine Tethys: the northern shelf (Gipf, Riniken and Rietheim), the Sub-Briançonnais basin (Creux de l'Ours), and the Lombardian basin (Breggia). The multi-proxy approach chosen (whole-rock and clay mineralogy, phosphorus, major and trace elements) shows that local environmental conditions modulated the response to the T-OAE across the Alpine Tethys. On the northern shelf and in the Sub-Briançonnais basin, high kaolinite contents and detrital proxies (detrital index, Ti, Zr, Si) in the T-OAE interval suggest a change towards a warmer and more humid climate coupled with an increase in the chemical weathering rates. In contrast, low kaolinite content in the Lombardian basin is likely related to a more arid climate along the southern Tethys margin and/or to a deeper and more distal setting. Redox-sensitive trace-element (V, Mo, Cu, Ni) enrichments in the T-OAE intervals reveal that dysoxic to anoxic conditions developed on the northern shelf, whereas reducing conditions were less severe in the Sub-Briançonnais basin. In the Lombardian basin well-oxygenated bottom water conditions prevailed. Phosphorus (P) speciation analysis was performed at Riniken and Creux de l'Ours. This is the first report of P speciation data for T-OAE sections, clearly suggesting that high P contents during this time interval are mainly linked to the presence of an authigenic phases and fish remains. The development of oxygen-depleted conditions during the T-OAE seems to have promoted the release of the organic-bound P back into the water column, thereby further sustaining primary productivity in a positive feedback loop.

1. Introduction

The Toarcian oceanic anoxic event (T-OAE, Early Jurassic) was marked by global warming, a perturbation of the carbon cycle, marine mass extinctions, and the widespread deposition of organic-rich strata, reflecting oceanic anoxia (Harries and Little, 1999; Jenkyns, 1988). The T-OAE coincides with the onset of the Karoo-Ferrar large igneous province (LIP) and the associated massive pulse in volcanic activity is currently thought to have initiated these environmental and climatic changes (Pálfy and Smith, 2000; Bond and Wignall, 2014; Burgess et al., 2015). The concomitant marked negative carbon-isotope excursion (CIE) recorded in the *tenuicostatum-falciferum* ammonite zones (or equivalents) was attributed to the injection of isotopically light carbon into the atmosphere and the ocean from (i) the input of thermogenic carbon dioxide (CO_2) produced by interaction of Karoo-Ferrar basalts and organic-rich sediments, (ii) the release of methane from the dissociation of marine clathrates, and (iii) the input of volcanogenic CO_2 (McElwain et al., 2005; Svensen et al., 2007; Kemp et al., 2011). The negative CIE is superimposed on a long-term positive trend, which was interpreted to reflect enhanced organic-carbon burial (Jenkyns, 1988). The negative CIE is recorded in marine carbonate carbon, and terrestrial and marine organic carbon in globally distributed settings, thereby confirming the global nature of the carbon-cycle perturbation and providing a better time marker for the T-OAE than solely the occurrence of organic-rich sediments (e.g., Röhl et al., 2001; Hesselbo et al., 2007; Suan et al., 2011, 2015; Gröcke et al., 2011; Caruthers et al., 2011; Kemp and Izumi, 2014; Reolid, 2014; Montero-Serrano et al., 2015; Bodin et al., 2016; Al-Suwaidi et al., 2016; Them II et al., 2017; Xu et al., 2017). Furthermore, global warming strengthened the hydrological cycle, resulting in increased continental weathering and hence

* Corresponding author.
E-mail address: alicia.fantasia@unil.ch (A. Fantasia).

https://doi.org/10.1016/j.gloplacha.2018.01.008
Received 12 November 2017; Received in revised form 22 December 2017; Accepted 8 January 2018
Available online 11 January 2018
0921-8181/

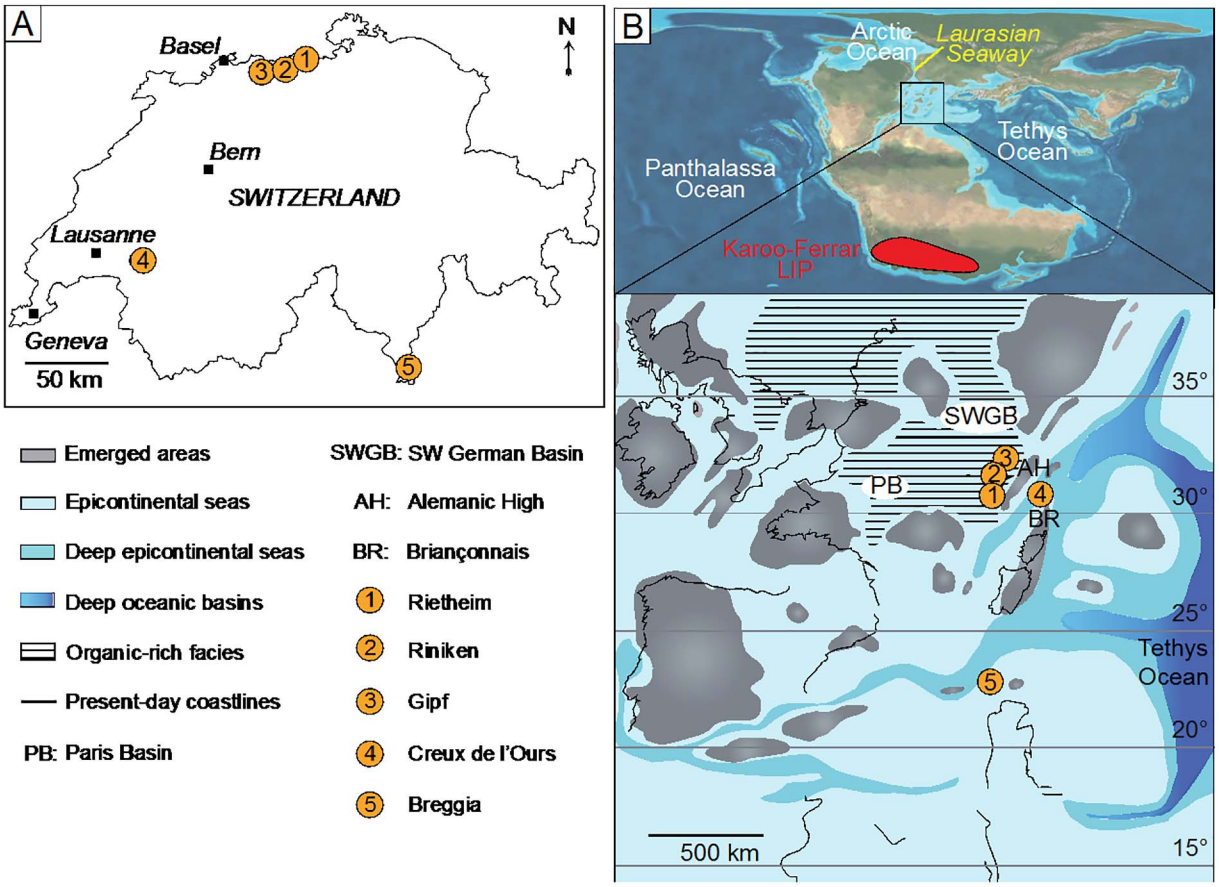

Fig. 1. A) Localisation of the studied sections in Switzerland. B) Paleogeographic map (modified from R. Blakey, http://cpgeosystems.com/euromaps.html) of the Early Toarcian showing the location of the Karoo-Ferrar LIP, the Laurasian Seaway, and a zoom on the western Tethys (after Thierry, 2000) with the location of the studied sections: Gipf, Riniken, Rietheim, Creux de l'Ours, and Breggia.

higher nutrient fluxes into the oceans (Cohen et al., 2004; Hermoso and Pellenard, 2014; Brazier et al., 2015; Fu et al., 2017). These conditions boosted primary productivity, which led to the development of oxygen-depleted conditions through organic-matter (OM) oxidation (Jenkyns, 2010). Hitherto, a major focus of T-OAE studies was on European restricted epicontinental basins and their organic-rich successions (e.g., Baudin et al., 1990; Jenkyns et al., 2001; Röhl et al., 2001; Hermoso et al., 2012). There, OM preservation was fostered by the thermohaline stratification caused by enhanced freshwater input and the southward flux of brackish water from the Laurasian Seaway (Bjerrum et al., 2001; Dera and Donnadieu, 2012). Relatively few studies, however, addressed the geographical extend of anoxic conditions, and the role of productivity and preservation in open-ocean successions (e.g., Gröcke et al., 2011; Them II et al., 2017).

In this study, a high-resolution multi-proxy study was performed on five Lower Toarcian successions located in Switzerland. They represent different paleogeographic settings across the Alpine Tethys, namely its northern shelf (Gipf, Riniken, Rietheim), the Sub-Briançonnais basin (Creux de l'Ours), and the Lombardian basin (Breggia) (Fig. 1). The main purposes of this study were to (i) trace the evolution of environmental and climate change during the T-OAE across the Alpine Tethys, (ii) evaluate the response to the T-OAE of successions deposited in different paleogeographic settings and at different paleodepths, (iii) better constrain the driving mechanisms in the development of oxygen-depleted conditions across the Alpine Tethys, and iv) better understand P behaviour during the T-OAE using P speciation analysis. This is the first report of P speciation values for T-OAE sections, which combined with the other proxies, brings new insight into the impact of the T-OAE and the role of local conditions in modulating the response to this global event.

2. Geological setting

The successions were selected according to their paleogeographic position and the presence of the negative CIE, which permits to trace the T-OAE interval across the Alpine Tethys (Fig. 1). This was provided by previous lithostratigraphic and biostratigraphic investigations performed by Rieber (1973), Wiedenmayer (1980), Tröster (1987), Matter et al. (1987), Kuhn and Etter (1994), Mettraux and Mosar (1989). In addition, a detailed study based on sedimentological features, nannofossil biostratigraphy, organic matter content, and stable isotopes was performed on these successions by Fantasia et al. (in review). This study highlights the presence of numerous stratigraphic gaps and condensed intervals related to the presence of winnowing events and sediment reworking during the T-OAE interval.

The sections of Gipf, Riniken (NAGRA borehole) and Rietheim are located in the northern Swiss Tabular Jura (Fig. 1A), canton Aargau, and were selected to characterise the northern shelf of the Alpine Tethys (Fig. 1B; Thierry, 2000). The Upper Pliensbachian interval is composed of phosphatic, glauconitic and fossil-rich marl and concretionary marly limestone. The Lower Toarcian interval is characterised by organic-rich laminated marl grading into bioturbated grey marl in the most expanded sections. The T-OAE interval is characterised by organic-rich laminated marl and shows evidences of episodic hydrodynamic conditions. At Gipf, the organic-rich laminated marl is topped by a condensed limestone bed. The *variabilis* and *thouarsense* zones (Middle and Upper Toarcian) are characterised by phosphatic concretionary marl with fossil accumulations (Fig. 2). Previous geochemical and whole-rock mineralogical investigations were recently performed for the Rietheim section by Montero-Serrano et al. (2015). Their results

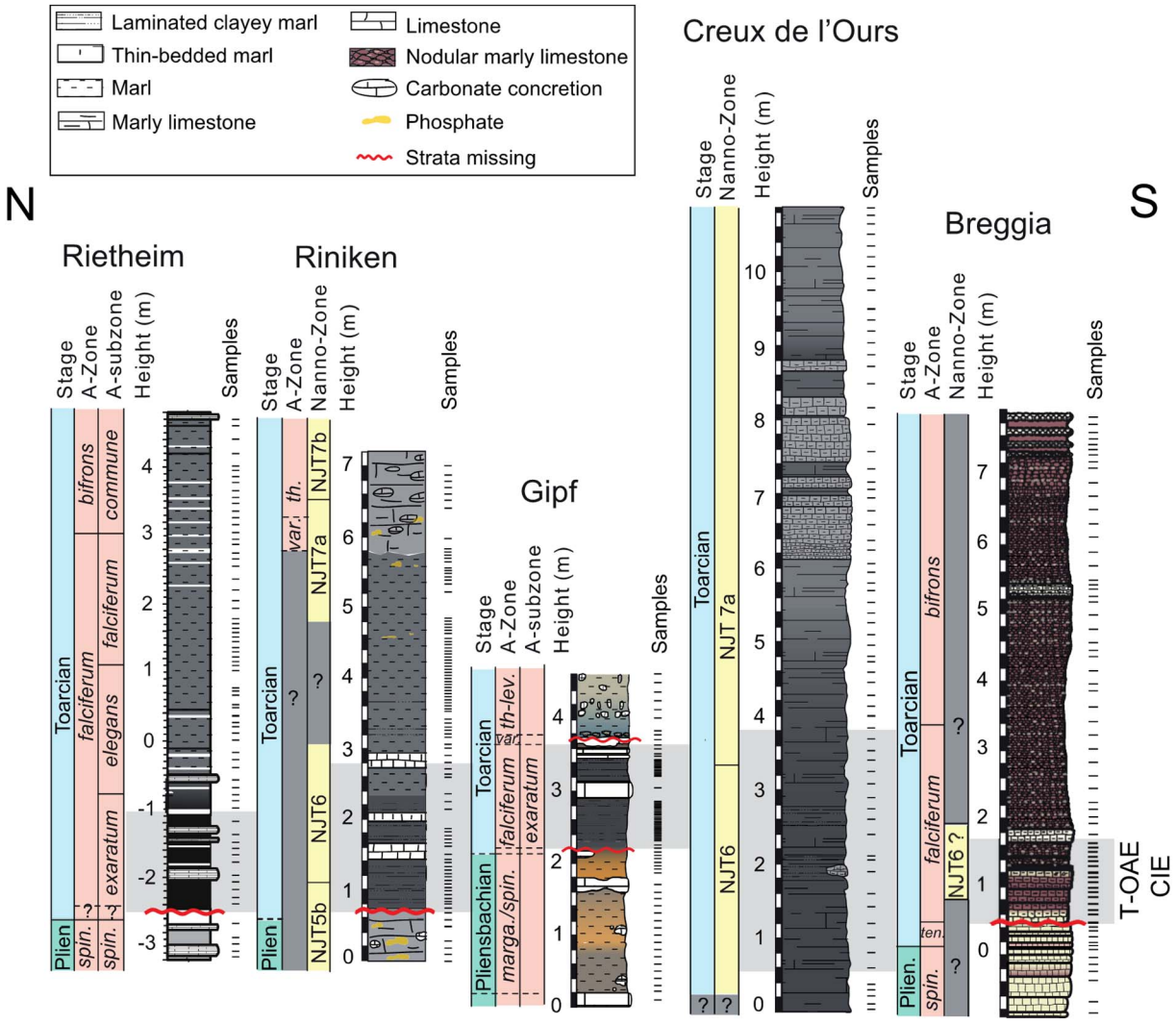

Fig. 2. Stratigraphic correlation between the studied sections and lithologies. The Rietheim section is from Montero-Serrano et al. (2015).

show that the T-OAE interval was characterised by anoxic (possibly euxinic) conditions, authigenic P, and an increase of the continental weathering. This was complement here by clay-minerals data to better constrain the role of climate conditions in modulating the environmental change. In addition, the sections of Gipf and Riniken were chosen in the same area to extend the research to a basin scale and to better understand the role of P during the T-OAE, as it was highlighted in studies on other OAEs (e.g., Mort et al., 2007; Westermann et al., 2013).

The Creux de l'Ours section is situated in the Préalpes Médianes Plastiques, canton Fribourg. The studied sediments were deposited in the Sub-Briançonnais basin, which was located to the NW of the Briançonnais micro-continent (Fig. 1B; Thierry, 2000). The Toarcian interval (Fig. 2) consists of grey thin-bedded hemipelagic marl and marly limestone including carbonate concretions formed around accumulations of ostracods and gastropods shells (*Coelodiscus minutus*). The T-OAE interval consists of thin-bedded marl and records short episodes of higher hydrodynamic conditions.

The Breggia section is exposed in the southern Alps, Canton Ticino, and was selected to characterise the hemipelagic realm (Fig. 1B; Thierry, 2000). The sediments from Breggia were deposited in the Monte Generoso subbasin, which was part of the Lombardian basin (Winterer and Bosellini, 1981). The Pliensbachian-Toarcian interval consists of yellow-grey to reddish bioturbated limestone, which grades into reddish nodular limestone and marl (Fig. 2). The T-OAE interval show organic-lean limestone, but the lower part of the interval is missing because of a stratigraphic gap (Wiedenmayer, 1980).

3. Methods

A detailed sampling was performed on the sections and whole-rock powders were obtained using an agate crusher. A total of 84 samples were collected at Gipf, 96 at Riniken, 65 at Creux de l'Ours and 74 at Breggia (Fig. 2). At Rietheim, 60 samples were selected for clay mineralogy analyses to complement previous geochemical study performed by Montero-Serrano et al. (2015). Mineralogical and geochemical analyses were conducted at the Institute of Earth Sciences of the University of Lausanne (Switzerland).

3.1. Whole-rock and clay mineralogy

Whole-rock and clay mineralogical analyses were performed on marl and limestone samples using a Thermo Scientific ARL X-TRA Diffractometer. The whole-rock mineralogical composition was semi-quantified using external standards and following the method described by Klug and Alexander (1974), Kübler (1987) and Adatte et al. (1996). For the clay minerals, the granulometric fraction < 2 μm was obtained following Kübler (1983) and Adatte et al. (1996). Clay samples were analysed after ethylene-glycol saturation. The kaolinite/(illite + chlorite) ratios (K/(I + C)) were calculated to trace the

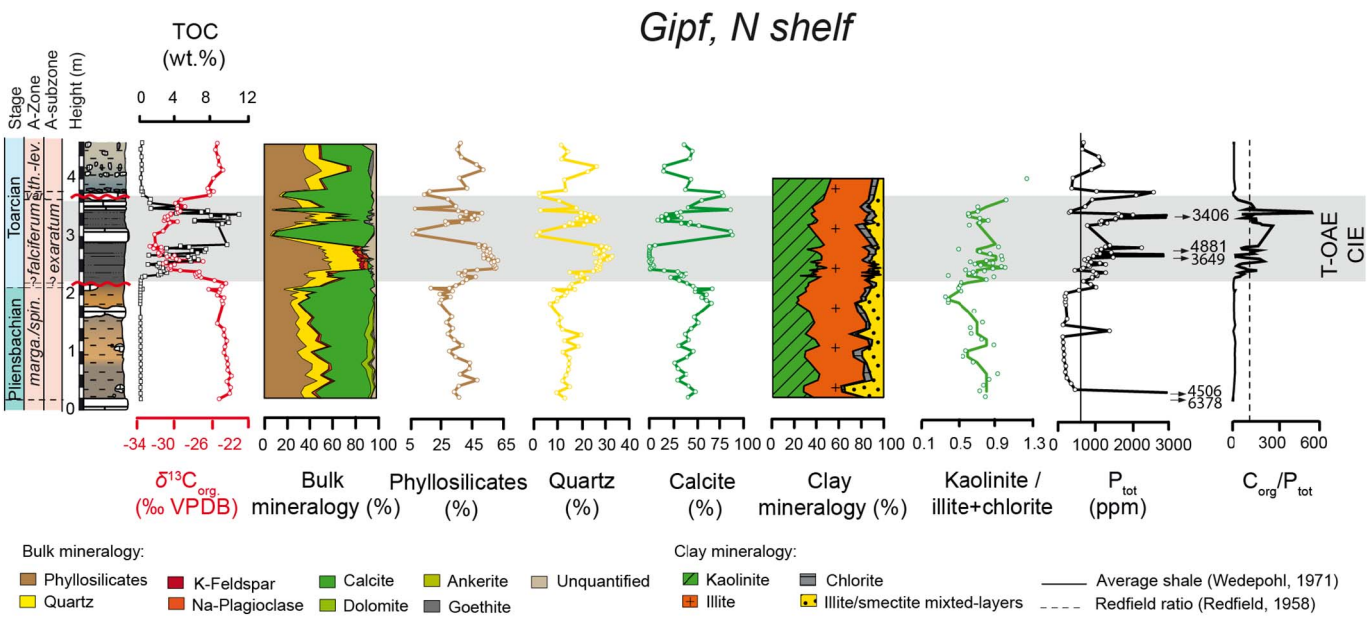

Fig. 3. Stratigraphic variations in the total organic carbon (TOC) content, organic-carbon isotopes ($\delta^{13}C_{org}$), whole-rock and clay mineralogy, total phosphorus (P_{tot}) content, and C_{org}/P_{tot} ratios along the Gipf section (northern shelf).

relationship between chemical and physical alteration (e.g., Duchamp-Alphonse et al., 2011). High K/(I + C) values suggest high chemical alteration related to more hydrolysing conditions under a warm and humid climate. The detrital index (DI) was calculated by dividing the sum of detrital minerals (quartz, phyllosilicates, Na-plagioclase, K-feldspar) by the calcite content (e.g., Adatte et al., 2002). High DI values indicate high input of terrigenous material and/or decreased carbonate production/increased dissolution.

3.2. Elemental geochemistry

Major (MEs; Si, Ti, Al, Ca, Na) and trace (TEs; Cu, Ni, Co, Cr, V, U, Mo, Zr) elements concentrations were determined by X-ray fluorescence spectrometry (XRFS), using a PANalytical PW2400 spectrometer. MEs were determined on fused lithium tetraborate glass disks, and TEs on pressed pellets of powered whole-rock samples mixed with Mowiol polyvinyl alcohol (2%). Analytical reproducibility monitored by replicate analyses of selected samples was lower than ± 5% for MEs and TEs. Analysis accuracy was assessed using international and in-house standard reference materials (TS1-Cement, TS3-Clay, TS4-Limestone, TS5-Marlstone, TS7-Sandstone, 372-Portland cement, 368-Dolomite).

A chemical index of alteration (CIA*), corrected for the carbonate content (McLennan et al., 1993; Fedo et al., 1995), was used to estimate the intensity of alteration related to paleoclimatic conditions (Nesbitt and Young, 1989).

$$CIA^* = [Al_2O_3/(Al_2O_3 + Na_2O + CaO^* + K_2O)] * 100$$

MEs and TEs were Al-normalised to correct for the dilution effect caused by variable proportions of the detrital mineral phases such as aluminosilicates that are of low mobility during diagenetic processes (Tribovillard et al., 2006). Al-normalisation is generally used when the coefficient of variation of Al concentration is not larger than that of other MEs and TEs (Riquier et al., 2006; Tribovillard et al., 2006). The detrital fluxes was evaluated based on Ti, Zr, and Si, and the oxygenation conditions with redox-sensitive TEs such as U, Mo, V, Ni and Cu.

Enrichment factors $EF_{element(X)} = (X/Al)_{sample} / (X/Al)_{average\ shale}$ (Brumsack, 2006; Tribovillard et al., 2006) were calculated to evaluate the relative enrichment of the element (X) compared to the average shale composition (Wedepohl, 1971). EF > 3 represents a detectable authigenic enrichment of an element over average shale concentrations, whereas EF > 10 represents a moderate to strong degree of authigenic enrichment (e.g., Tribovillard et al., 2006; Algeo and Tribovillard, 2009).

3.3. Phosphorus

To extract total phosphorus (P_{tot}), 1 mL of 1 M $Mg(NO_3)_2$ was added to 100 ± 5 mg of powdered whole-rock sample and then placed in an oven at 550 °C during 2 h30. After cooling 10 mL of HCl (1 N) was added. The preparation was then placed on a shaker for 16 h in order to liberate the P_{tot}. Samples were then filtered (0.45 µm) and analysed using the ascorbic acid method (Eaton et al., 1995). In addition, the SEDEX sequential extraction method developed by Ruttenberg (1992) and adapted by Mort et al. (2007) was used to quantify the authigenic (P_{auth}), detrital (P_{det}) and organic (P_{org}) P phases. P concentrations (ppm) were measured using an UV/Vis Perkin Elmer Spectrophotometer. C_{org}/P_{org} and C_{org}/P_{tot} (Redfield) molar ratios were calculated (C_{org} = total organic carbon).

4. Results

4.1. Whole-rock mineralogy and clay mineralogy

At Gipf, phyllosilicates (17–61%), calcite (3–77%) and quartz (2–26%) are the dominant minerals in the clayey marl and marl, whereas calcite (78–88%) dominates the limestone beds (Fig. 3). Phyllosilicates and quartz show a decreasing trend towards the Pliensbachian-Toarcian boundary followed by an abrupt increase at the base of the CIE interval, which coincides with a drop in calcite content to 0.3%. The presence of goethite throughout the section is likely related to the oxidation of pyrite (Nordstrom, 1982). Clay-mineral assemblages consist mainly of kaolinite (21–52%), illite (34–58%), chlorite (1–11%) and illite/smectite mixed-layers (2–35%) (Fig. 3). Kaolinite and K/(I + C) show a decrease towards the Pliensbachian-Toarcian boundary. This is followed by a marked increase in kaolinite (up to 49%) and K/(I + C) at the onset of the negative CIE. Then, a transient decrease is observed in the upper portion of the negative CIE interval below a second increase in the *thouarsense-levesquei* zones (Upper Toarcian) (Fig. 3).

At Riniken, phyllosilicates (18–55%), calcite (8–70%), quartz (4–31%) dominate the whole-rock composition in the clayey and marly

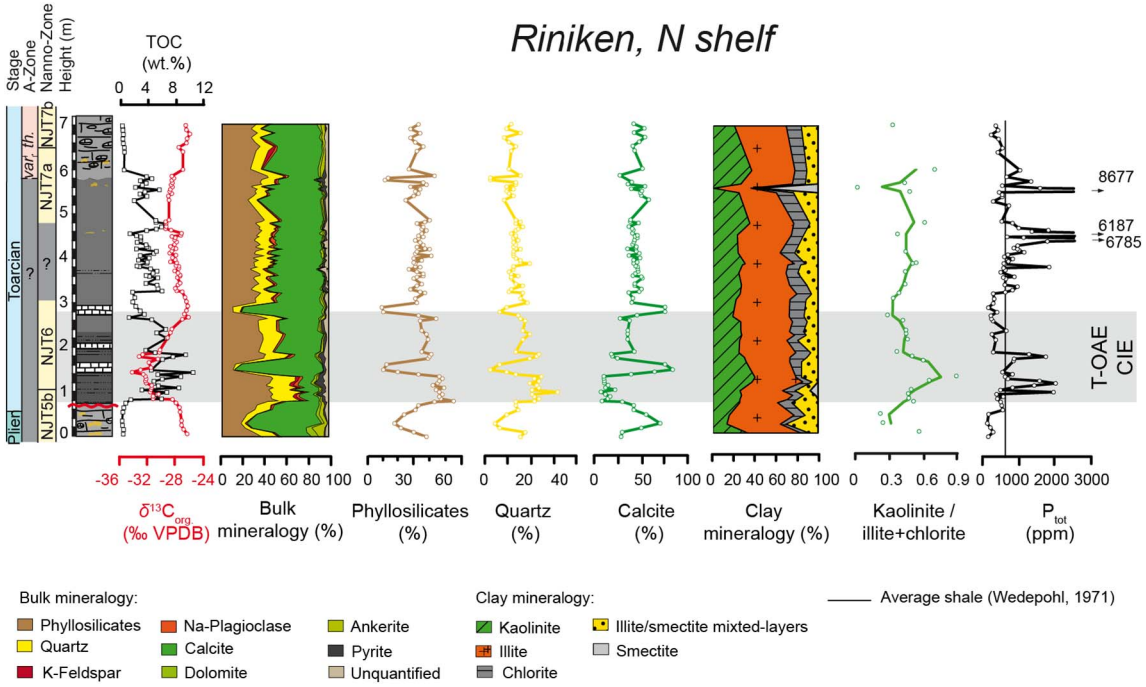

Fig. 4. Stratigraphic variations in the total organic carbon (TOC) content, organic-carbon isotopes ($\delta^{13}C_{org}$), whole-rock mineralogy, clay-mineral assemblages, and total phosphorus (P_{tot}) content at Riniken (northern shelf).

intervals, whereas calcite is the dominant mineral (64–83%) in the limestone beds. Phyllosilicates and quartz show a decrease towards the Pliensbachian-Toarcian boundary interval, whereas calcite increases. A sharp decrease in the calcite content to 8% is observed at the base of the CIE interval, whereas phyllosilicates and quartz increase (up to 55% and 31%, respectively). The clay fraction is mainly composed of kaolinite (13–40%), illite (33–62%), chlorite (3–19%) and illite/smectite mixed-layers (5–31%) (Fig. 4). Smectite is present in low amounts at the base of the section (at 0.90 m: 2% and at 1.05 m: 8%). A peak in smectite is observed at 5.6 m (56%) and corresponds to a lithological change. A marked increase in kaolinite and K/(I + C) is observed at the base of the CIE interval, followed by a decrease in the upper portion of this interval and a long-term increasing trend section upward (Fig. 4).

At Rietheim, the clay fraction is dominated by kaolinite (16–41%), illite (29–56%), chlorite (5–24%) and illite/smectite mixed-layers (3–34%) (Fig. 5). Kaolinite and K/(I + C) increase at the base of the CIE interval. A transient decrease in kaolinite is observed in the upper portion of the CIE, followed by a long-term increase up to the top of section.

At Creux de l'Ours, the Lower Toarcian marl mainly consists of calcite (15–51%), phyllosilicates (28–50%) and quartz (10–29%), with lower proportions of K-feldspar, Na-plagioclase, dolomite and ankerite (Fig. 6). The calcite content shows the lowest values within the CIE interval (mean is 27%) and then gradually increases section upward. This is inversely correlated with phyllosilicates and quartz, both having the highest values within the CIE interval (up to 50% and up to 49%, respectively). The clay-mineral assemblage consists predominantly of illite (30–56%) and kaolinite (12–36%), and in lower proportions of chlorite (2–15%), smectite (0–19%) and illite/smectite mixed-layers (6–26%) (Fig. 6). The negative CIE is marked by an increase in kaolinite (from 16% to 35%) and K/(I + C). This is followed by a decrease in the upper portion of the CIE and a long-term increase section upward.

At Breggia, the Pliensbachian-Toarcian interval is dominated by calcite (40–86%), phyllosilicates (5–34%) and quartz (3–20%) (Fig. 7). Calcite is inversely correlated with phyllosilicates and quartz. Quartz and phyllosilicates increase just above the stratigraphic gap (*tenuicostatum-falciferum* zones). This is followed by a transient decrease and a long-term increase from the uppermost part of the CIE (from 1.6 m)

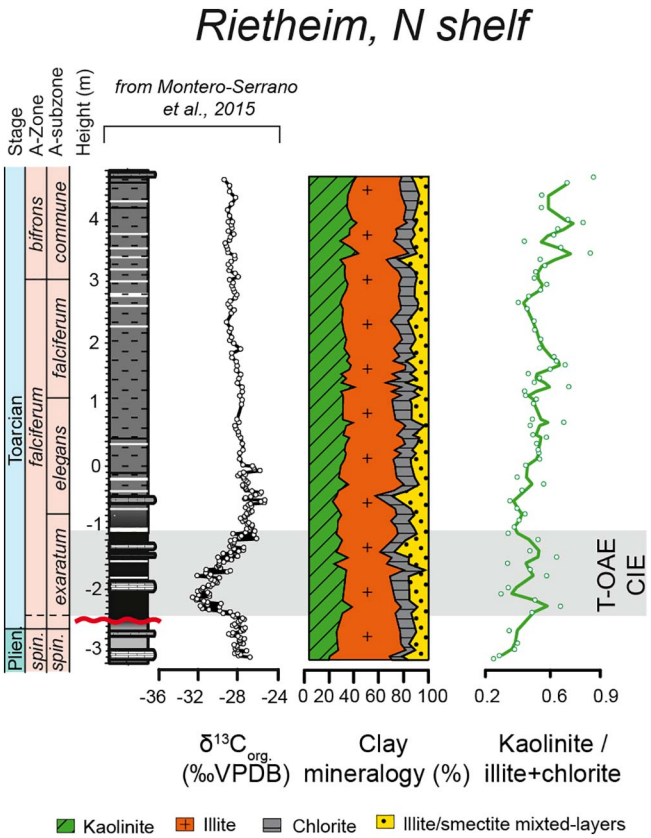

Fig. 5. Clay-mineral distribution and organic-carbon isotopes ($\delta^{13}C_{org}$) at Rietheim (northern shelf).

section upward. The clay fraction is dominated by illite and smectite, with lower proportions of chlorite, kaolinite and illite/smectite mixed-layers. Smectite and illite dominate the assemblage (up to 60 and 45%, respectively) in the CIE interval, whereas kaolinite is nearly absent

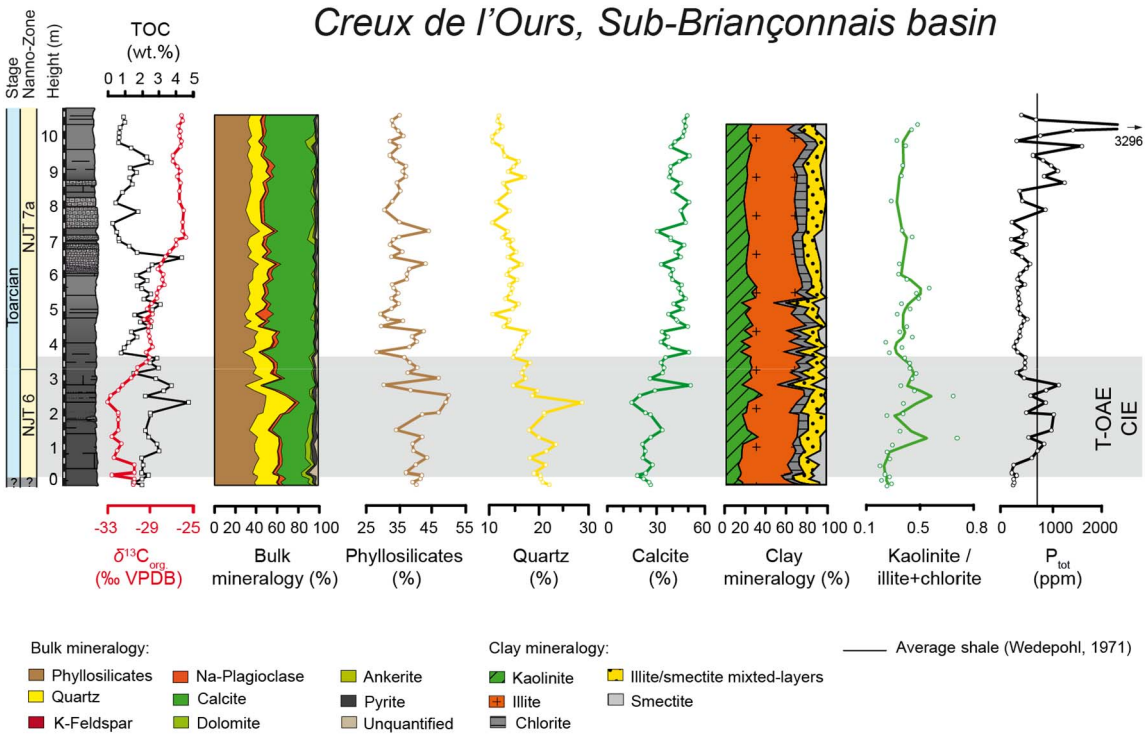

Fig. 6. Stratigraphic variations in the total organic carbon (TOC) content, organic-carbon isotopes ($\delta^{13}C_{org}$), whole-rock mineralogy, clay-mineral assemblages, and total phosphorus (P_{tot}) content at Creux de l'Ours (Sub-Briançonnais basin).

(0–2%). The K/(I + C) ratio is low and increases in the upper portion of the CIE and onwards, together with kaolinite (up to 20%) (Fig. 7).

4.2. Phosphorus

At Gipf, P_{tot} content is low (150–480 ppm) in the Upper Pliensbachian interval except for two peaks of > 1000 ppm (Fig. 3). The CIE interval is marked two main P_{tot} increases (up to 4880 ppm and 3406 ppm, respectively) and high C_{org}/P_{tot} ratios (up to 540 ppm). This is followed by a return to background concentrations in the upper portion of the CIE interval (mean: 308 ppm) and a sharp increase to 2600 ppm in the condensed limestone bed at 3.7 m (Fig. 3).

At Riniken, P_{tot} increases up to 2370 ppm at the base of the CIE interval (Figs. 4 and 8), followed by a decrease (180–760 ppm) in the upper part of this interval. Two intervals of very high values (up to 6785 and 8677 ppm, respectively) are observed in the upper part of the

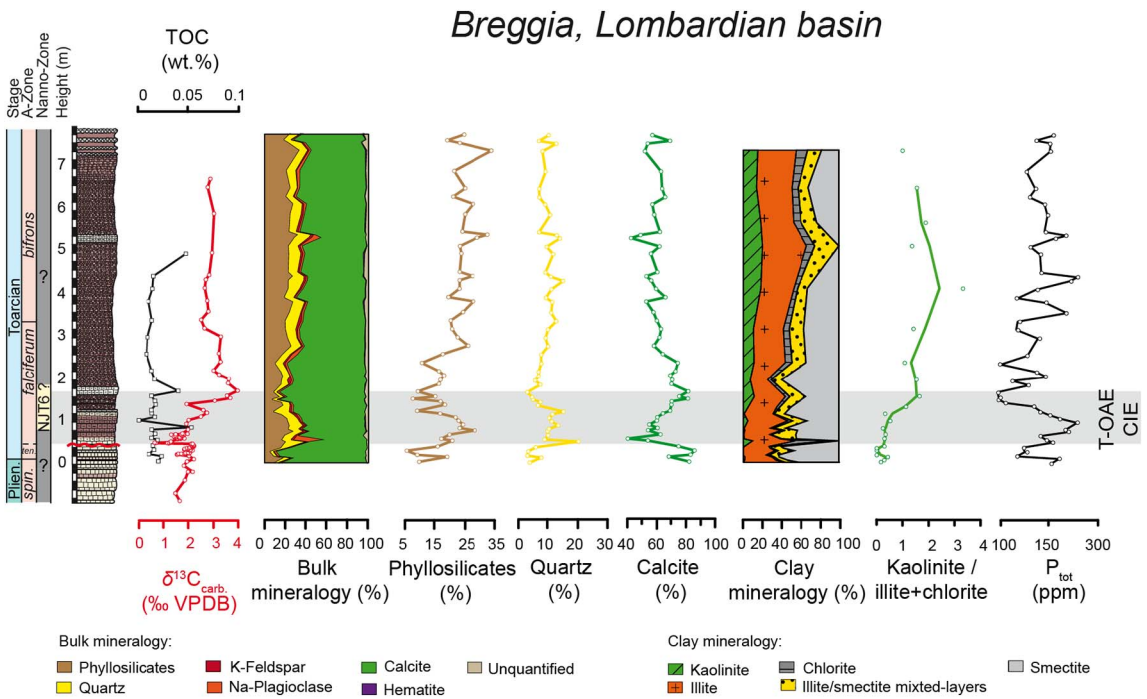

Fig. 7. Stratigraphic variations in the total organic carbon (TOC) content, organic-carbon isotopes ($\delta^{13}C_{org}$), whole-rock and clay mineralogy, and the total phosphorus (P_{tot}) content along the Breggia section (Lombardian basin).

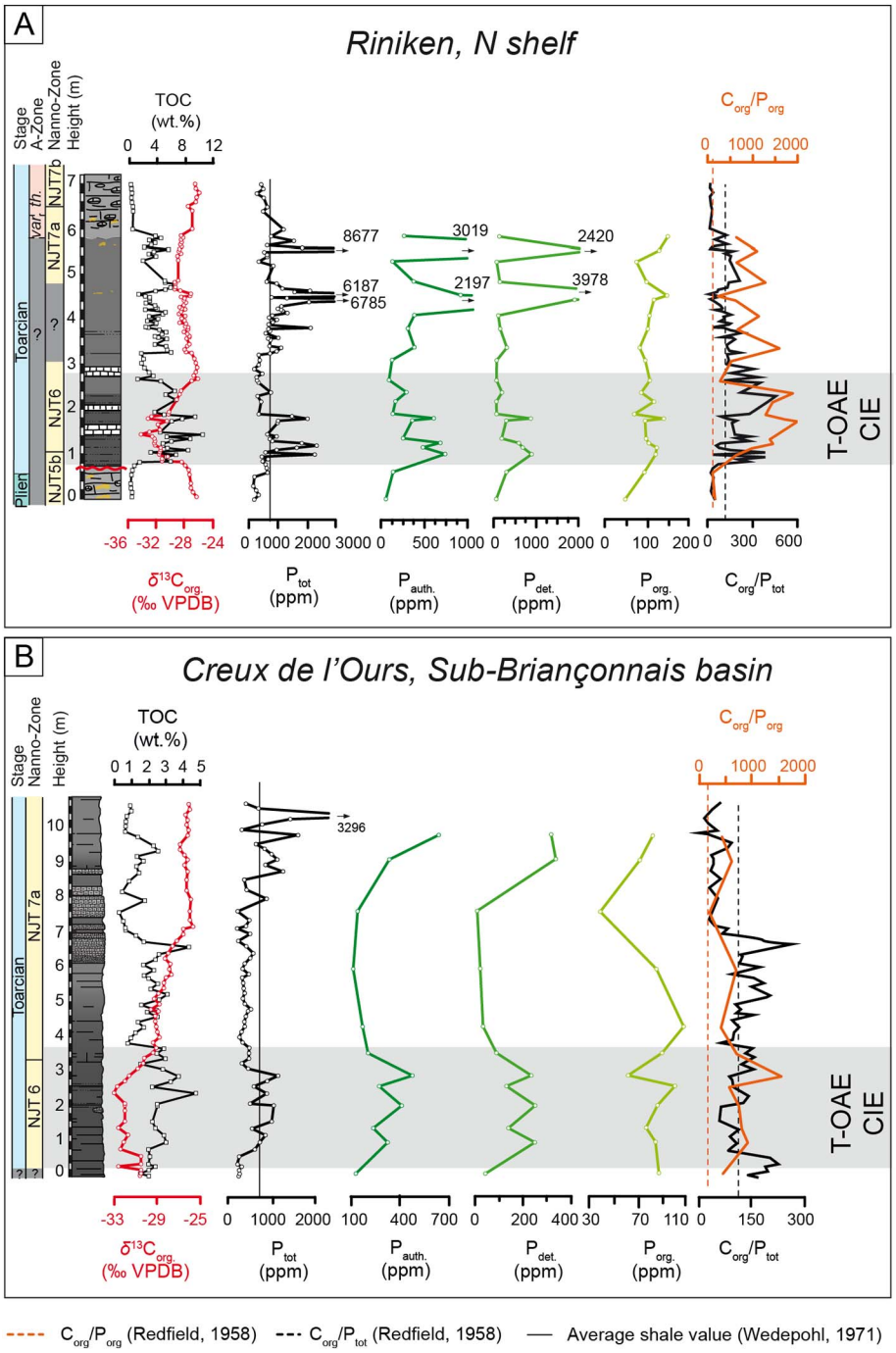

Fig. 8. Phosphorus speciation ($P_{det.}$, $P_{auth.}$, $P_{org.}$) at (A) Riniken and (B) Creux de l'Ours, plotted against the organic-carbon isotopes ($\delta^{13}C_{org}$) and the total organic carbon (TOC) content.

section and correspond to phosphatic crusts and concretions in the marly limestone.

The main P phases are P_{auth} (mean: 520 ppm), and P_{det} (mean: 633 ppm), whereas P_{org} shows lower values (mean: 106 ppm) (Fig. 8A). P_{auth} and P_{det} show trends similar to P_{tot} (r^2 = 0.88 and 0.80, respectively). P_{org} increases at the onset of the CIE interval and then remains relatively constant section upward. The C_{org}/P_{tot} and C_{org}/P_{org} ratios show parallel trends and reach maximum values in the CIE interval (449 and 2000, respectively) (Fig. 8A).

At Creux de l'Ours, the base of the CIE interval shows an increase in P_{tot} values (up to 1150 ppm), followed by a return to background values (236–474 ppm) in the upper part of this interval (Figs. 6 and 8B). Maximal values (3296 ppm) are reached in the upper part of the section. P_{auth} (mean: 283) and P_{det} (mean: 154 ppm) are the main P phases and follow P_{tot} distribution (Fig. 8B). P_{org} is a minor phase (mean: 82 ppm) and shows higher values across the CIE interval, followed by generally lower values above this interval. C_{org}/P_{tot} ratios are low and show constant values (mean: 127) within the CIE interval. The C_{org}/P_{org} ratio shows higher values than C_{org}/P_{tot} and maximal values (1550) are reached in the CIE interval (Fig. 8B).

At Breggia, P_{tot} values are low (100–260 ppm) and show a slight increase (up to 260 ppm) within the CIE interval (Fig. 7). This is followed by a decrease in the upper portion of this interval and a long-term increasing trend section upward.

4.3. Major and trace element abundances

At Gipf, Si, Ti, and Zr show a good correlation with Al (r^2 = 0.97,

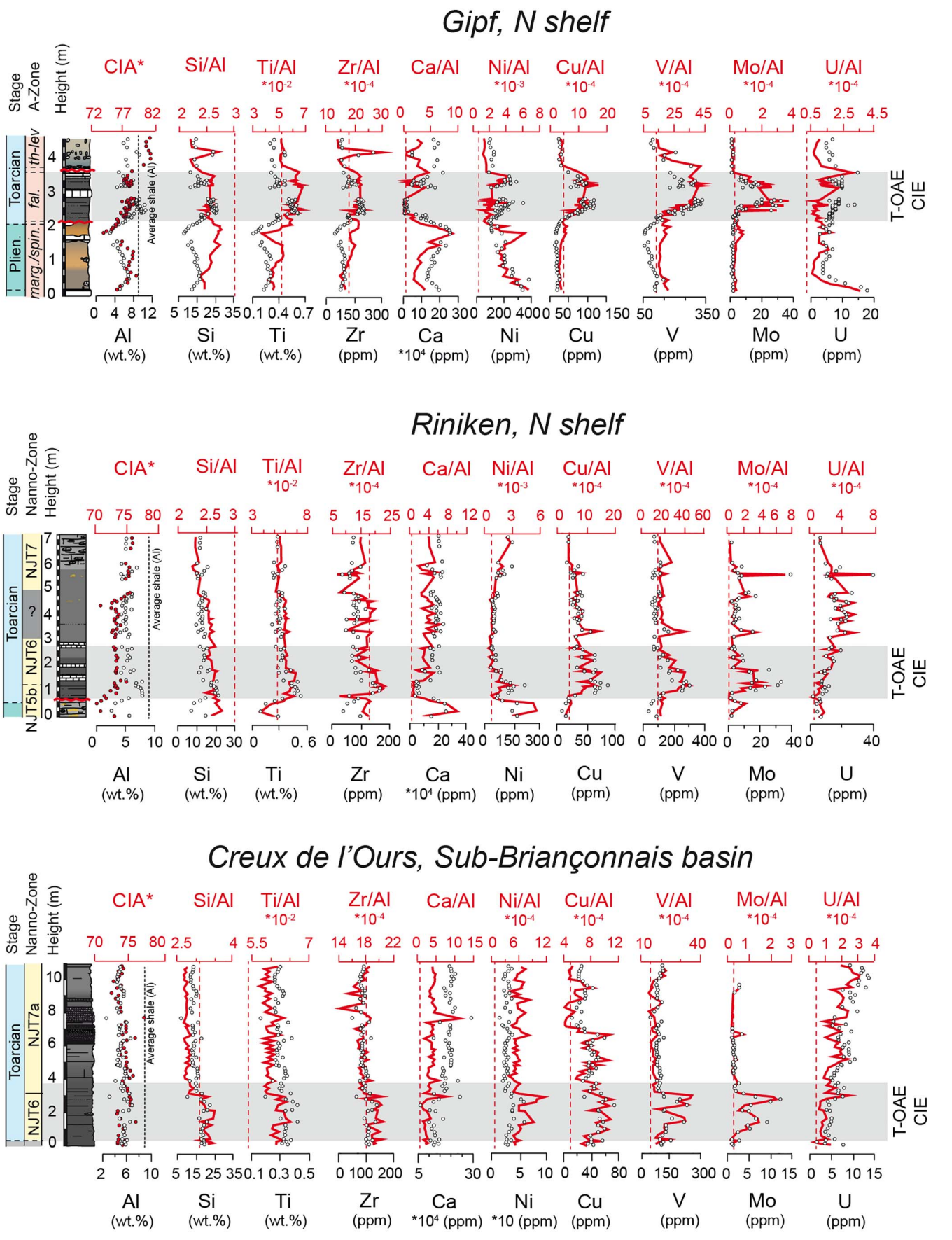

(caption on next page)

Fig. 9. Stratigraphic evolution of major and trace elements for the sections of Gipf, Riniken and Creux de l'Ours. The CIA* values are plotted against the Al trend. The data are shown in absolute (wt% and ppm; black dots) and Al-normalised (red lines) contents. (For interpretation of the references to colour in this figure legend, the reader is referred to the web version of this article.)

0.91, 0.90, respectively) and exhibit trends similar to the CIA* (Fig. 9). They all show a sharp increase just below the Pliensbachian-Toarcian boundary and maximum values in the CIE interval, followed by a return to background values. Ti/Al and Zr/Al display their highest values in the CIE interval, whereas Si/Al shows relatively stable values along the section (Fig. 9). Cu/Al, V/Al and Mo/Al show the highest values in the CIE interval, followed by a return to background values (Fig. 9).

Ni/Al and U/Al show a decreasing trend below the Pliensbachian-Toarcian boundary, followed by a slight increase at the onset of the CIE and then a return to lower values after this interval (Fig. 9).

At Riniken, Si, Ti, and Zr are moderately correlated with Al (r^2 = 0.96, 0.93, 0.59). Ti/Al, Zr/Al and CIA* reach maximum values at the base of the CIE interval (Fig. 9). Si/Al shows the highest values below the Pliensbachian-Toarcian boundary and then a decreasing trend section upward. Cu/Al, V/Al and Mo/Al reach maximum values at the base of the CIE interval (Fig. 9). Ni/Al shows the highest values in the Upper Pliensbachian interval and a sharp decrease just below the CIE interval. A slight increase is observed at the base of the CIE, followed by a return to lower values section upward. U/Al shows a gradual increase from the base to the top of the section, reaching its maximum value above the CIE interval.

At Creux de l'Ours, Si, Ti, and Zr are highly correlated with Al (r^2 = 0.78, 0.96, 0.87, respectively) and display a trend similar to the CIA*. Si/Al, Ti/Al, Zr/Al and CIA* show the highest values within the CIE interval and a decreasing trend section upward (Fig. 9). Ni/Al, Cu/Al, V/Al, Mo/Al and U/Al show the highest values within the CIE interval. Ni/Al, V/Al and Mo/Al display a sharp decrease in the second part of the CIE interval, whereas Cu/Al exhibit more fluctuating values. U/Al shows an increase from the base to the top of the section (Fig. 9).

5. Discussion

5.1. Clay minerals

5.1.1. Preservation of the primary clay minerals

The late diagenetic effect on the primary clay mineral assemblage must be evaluated before any paleoenvironmental interpretation (e.g., Chamley, 1989; Kübler and Jaboyedoff, 2000). At Gipf, Riniken and Rietheim (northern shelf), T_{max} values up to 440 °C and the absence of smectite suggest a moderate diagenetic overprint, because smectite commonly transforms into illite when burial depth reaches about 2000 m and/or when T_{max} values reach 430–440 °C (Burtner and Warner, 1986; Chamley, 1989). In these successions, burial depth may have been underestimated and the geothermal gradient higher due to the proximity to the Rhine graben (Todorov et al., 1993). At Creux de l'Ours (Sub-Briançonnais basin) and Breggia (Lombardian basin), the presence of smectite and the low abundance of illite/smectite mixed-layers indicate a weak diagenetic overprint and/or neoformation of smectite. Indeed, the presence of radiolarians in these more open-marine sections may have been a source of dissolved Si, which was subsequently involved in the precipitation of authigenic smectite (Chamley, 1989). The weak influence of burial diagenesis is supported by T_{max} values up to 435 °C and 439 °C, respectively (Deconinck and Bernoulli, 1991; Fantasia et al., in review).

In all studied sections, the presence of kaolinite suggests that the diagenetic overprint was however not too strong and variations in the clay-mineral assemblages likely reflect a primary paleoenvironmental signal. K/(I + C) ratios combined with CIA* values were used to trace changes in hydrolysing conditions and humidity variations.

5.1.2. Paleoclimatic conditions

At Gipf, Riniken, Rietheim (northern shelf) and Creux de l'Ours (Sub-Briançonnais basin), K/(I + C) ratios display comparable trends (Fig. 10). The low K/(I + C) ratios in the Upper Pliensbachian intervals may indicate a relatively cool to temperate and/or dry climate (Chamley, 1989; Velde, 1995). This is supported by the relatively low CIA* values compared to the Toarcian interval. The Late Pliensbachian was marked by a regression (Haq et al., 1987; Hardenbol et al., 1998; Haq, 2017), which supports the interpretation that the decrease in kaolinite is likely related to paleoclimatic conditions rather than to sea-level change. The increase of K/(I + C) and CIA* values at the onset of the CIE, suggests a shift towards a warmer and more humid climate (Thiry, 2000), which led to increased hydrolysing conditions on the surrounding landmasses during the T-OAE (Fig. 10). This major change in the clay-mineral assemblage was also observed in other NW European basins (Dera et al., 2009; Hermoso and Pellenard, 2014; Bougeault et al., 2017).

The distal paleogeographic position of the sections of Creux de l'Ours (Sub-Briançonnais basin) and Breggia (Lombardian basin) (Thierry, 2000) coupled with the Early Toarcian transgression (Haq, 2017), likely interfered with the distribution of larger kaolinite clay (e.g., Gibbs, 1977; Adatte et al., 2002; Godet et al., 2008). This could explain lower kaolinite contents in the deepest and more distal settings. In addition, at Breggia, a drier belt along the southern Tethyan margin during the T-OAE (Van de Schootbrugge et al., 2005) may have been responsible for the low K/(I + C) ratios owing to low hydrolysing conditions. The predominance of smectite in the CIE interval most likely reflects the weathering of soils developed on a distant landmass under a semi-arid climate with alternating humid and dry seasons (Singer, 1984; Chamley, 1989). The high content in illite suggests a nearby clastic source; such may have been the Gozzano High, located to the west of the Lombardian basin, and uplifted during the latest Triassic-Early Jurassic (Bernoulli and Ulmer, 2016). Deconinck and Bernoulli (1991) assigned the diversity of the clay-mineral assemblages at Breggia to the weathering of various parent materials, including soils and crystalline basement. Above the CIE interval, the gradual increase in kaolinite relative to smectite is likely related to a shift towards warmer and more humid conditions rather than to sea-level rise, which would have rather lead to an increase in smectite contents (Figs. 7 and 10). This trend is similarly observed in the other studied sections and coincides with high CIA* values. Therefore, the hydrolysing conditions, induced by the warm and humid climate initiated during the Early Toarcian, appear to have prevailed well after the CIE interval in the Alpine Tethys (up to the *bifrons* Zone; Dera et al., 2009).

5.2. Change in continental weathering

At Gipf, Riniken (northern shelf) and Creux de l'Ours (Sub-Briançonnais basin), the CIE interval is marked by an increase (or the highest values) in the CIA*, detrital index and detrital elements (Figs. 9 and 10). This suggests that the climate shift towards warmer and more humid climate (high kaolinite) increased the weathering rate in the nearby source areas during the T-OAE. The increase in the detrital index is thus likely related to (i) the increase in continental runoff, (ii) significant reworking during the early transgressive phase, (iii) a decrease in the calcite content (acidification) due to the injection of greenhouse gases into the atmosphere and the ocean (e.g., Suan et al., 2008; Trecalli et al., 2012). High Ti/Al and Zr/Al during the CIE may be related to enhanced detrital supply from fluvial discharge, since these elements are generally associated with heavy mineral grains (ilmenite, rutile, zircon) and/or to an increase in eolian supply (Riquier et al.,

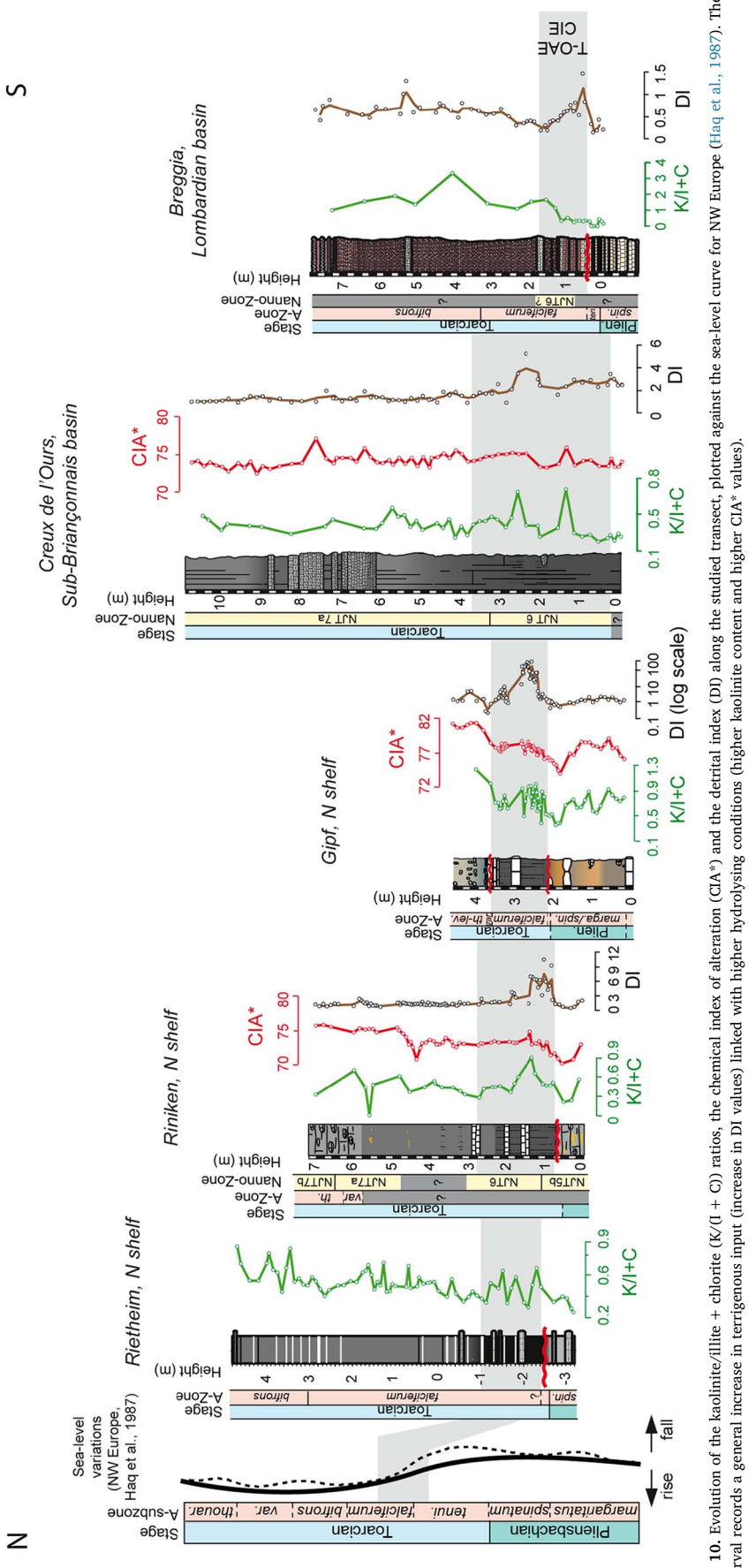

Fig. 10. Evolution of the kaolinite/illite + chlorite (K/(I + C)) ratios, the chemical index of alteration (CIA*) and the detrital index (DI) along the studied transect, plotted against the sea-level curve for NW Europe (Haq et al., 1987). The CIE interval records a general increase in terrigenous input (increase in DI values) linked with higher hydrolysing conditions (higher kaolinite content and higher CIA* values).

2006). Ti and Zr might also have been enriched relative to more labile elements due to the stronger hydrolysing conditions. These results are in good agreement with other studies from the European areas (e.g., Cohen et al., 2004; Hermoso and Pellenard, 2014; Brazier et al., 2015). Higher hydrolysing conditions favoured higher nutrient fluxes into the basins, ultimately boosting primary productivity and the development of oxygen-depleted conditions (Jenkyns, 2010). It is not excluded that the deep and more distal setting of the Creux de l'Ours section modulated detrital input and nutrient fluxes.

At Breggia (Lombardian basin), the low hydrolysing conditions (low kaolinite) recorded in the upper part of CIE coupled with the deeper and more distal setting likely limited detrital input. The slight increase in the detrital index in this interval is rather linked to condensation (distal setting and carbonate dissolution) rather than to higher detrital input. Indeed, the T-OAE was marked by a general biocalcification crisis in pelagic and benthic communities, which was attributed to eutrophication and changes in ocean chemistry (e.g., Mattioli et al., 2008; Trecalli et al., 2012; Reolid et al., 2014; Ferreira et al., 2017). This led to the near disappearance of shallow-water platforms and the decrease in carbonate accumulation in the deepest parts of the basins (Blomeier and Reijmer, 1999; Mattioli et al., 2009; Trecalli et al., 2012). Therefore, condensation related to the decrease in carbonate production might have been more important in carbonate-dominated settings like at Breggia.

5.3. Redox conditions

At Gipf, Riniken (northern shelf) and Creux de l'Ours (Sub-Briançonnais basin), the increasing trends in redox-sensitive TEs (V, Mo, Cu, Ni) coupled with low to modest EFs (Gipf: 1–13; Riniken: 0.5–21; Creux de l'Ours: 0.6–12) during the T-OAE interval indicate a shift towards oxygen-depleted conditions (Figs. 9 and 12A). These elements tend to be less soluble under reducing conditions, and depend on the flux of OM delivered to the sediments and the formation of sulphides (mainly pyrite), whose accumulation is largely controlled by the oxygenation conditions of the sedimentary environment (Riquier et al., 2006; Tribovillard et al., 2006; Calvert and Pedersen, 2007). The Mo-TOC scatterplot indicate that sediments were deposited under dysoxic to anoxic conditions at Gipf and Riniken and mostly under dysoxic conditions at Creux de l'Ours in the T-OAE interval (Fig. 11A). This is supported by the absence of genuine laminated organic-rich sediments in the latter. In addition, sedimentological features (e.g., obliquely-bedded laminae and homogeneous mud layers containing rip-up clasts) observed in these successions (Fantasia et al., in review) indicate that short episodes of winnowing and sediment reworking likely precluded the development of strong and persistent bottom-water anoxia in these sections.

The poor correlation of Ni, Cu, V and Mo with TOC and Al indicates that these elements were mainly enriched through redox processes (Fig. 11B). EFs of V, Mo, Ni and Cu are lower than the EFs from sites characterised by strong anoxia (e.g., Brumsack, 2006), supporting our interpretation that dysoxic to anoxic conditions developed during the T-OAE interval rather than strong anoxia or euxinia (Fig. 12B). At Gipf, Riniken and Creux de l'Ours, U shows a trend different to the other redox-sensitive TEs, especially above the CIE interval. This may be due to variability in the sedimentation-accumulation rate (Wignall and Maynard, 1993) and/or to adsorption onto authigenic phosphate (Abed and Sadaqah, 2013).

At Gipf, Riniken and Creux de l'Ours, Ni/Al and Cu/Al show a slight to sharp increase in the T-OAE interval, which coincides with an interval of high OM content (Fig. 9). These elements are generally delivered and retained in the sediment in association with OM under reducing conditions (Algeo and Maynard, 2004; Tribovillard et al., 2006). Therefore, the increase in Ni and Cu within the T-OAE likely indicates a higher OM flux and thus potentially higher productivity. High Ni concentrations appear to be coupled with high Ca values in the marly limestone from the Pliensbachian and Upper Toarcian, likely due to the preferential precipitation of Ni in carbonate complex (Tribovillard et al., 2006).

At Breggia (Lombardian basin), the degree of oxygenation is inferred from sedimentological observations. Even if the lower part of the negative CIE is missing due to a stratigraphic gap, the presence of abundant bioturbation and the absence of OM in the interval showing the return to more positive values in the CIE indicate that oxic conditions prevailed (Fantasia et al., in review).

5.4. Insights from phosphorus

At Gipf, Riniken (northern shelf) and Creux de l'Ours (Sub-Briançonnais basin), high P_{tot} values coupled with high TOC values are recorded in sediments deposited under dysoxic to intermittently anoxic conditions (Fig. 13). Mesozoic OAEs generally show a drastic decrease in P_{tot} because P is strongly dependent on redox conditions at the sediment-water interface and generally released to the water column under reducing conditions (e.g., Van Cappellen and Ingall, 1994; Föllmi, 1996; Mort et al., 2007). Consequently, P may increase primary productivity, expand the oxygen-minimum zone and reinforce the sinking flux of organic carbon in a positive feedback loop (Van Cappellen and Ingall, 1994; Filippelli and Delaney, 1996; Mort et al., 2007). On the other hand, under oxic conditions, part of the remineralised organic P may be trapped in the sediment mainly through authigenesis and adsorption on clay minerals and Fe-oxyhydroxides (Slomp et al., 1996; Algeo and Ingall, 2007).

At Riniken and Creux de l'Ours, C_{org}/P_{org} ratios higher than the Redfield ratio (106:1; Redfield, 1958) in the CIE interval suggests that the retention capacity of P in OM was very low and that preserved OM was depleted in P relative to carbon. P can be laterally transferred into authigenic P during diagenesis and thus C_{org}/P_{org} ratios are commonly used (Anderson et al., 2001; Algeo and Ingall, 2007). C_{org}/P_{tot} higher than C_{org}/P_{org}, and both slightly to markedly higher than the Redfield ratio in the CIE interval (Fig. 8) suggest a lateral transfer of organic-bound P into an authigenic phase and/or the release of P back into the water column. It appears from the thin-sections analysis that the "authigenic" P is mostly related to fish remains (biogenic P), which may have been converted into more stable carbonate fluorapatite (Schenau and de Lange, 2000). However, P authigenesis cannot be totally excluded. High P_{det} contents observed at Riniken (boundary between NJT6 and NJT7a nannofossil zones) are related to the presence of authigenic P crusts. Indeed, P_{det} may correspond to an authigenic phase, which underwent subsequent recrystallisation (e.g., Filippelli and Delaney, 1996; Föllmi et al., 2005).

At Riniken, P_{det} is moderately correlated with the detrital index ($r^2 = 0.42$), Ti ($r^2 = 0.48$), Zr ($r^2 = 0.56$) at the base of the CIE interval. This correlation is not observed at Creux de l'Ours. The paleogeographic position of the Riniken section close to large landmasses coupled with the increase in hydrolysis in the source areas (high CIA*) likely favoured high P input from the continent, boosting primary productivity (Föllmi, 1995; Tyrell, 1999). In addition, P_{org} recycling (low P_{org} burial efficiency) under reducing conditions during the T-OAE was likely efficient creating a positive feedback loop sustaining primary productivity, as is also known from other OAEs. Therefore, the decrease in P_{org} burial efficiency at Riniken and Creux de l'Ours during the T-OAE likely helped to sustain oxygen depleted conditions.

At Breggia (Lombardian basin), low P_{tot} values in the upper portion of the CIE may be related to the (i) large distance away from large landmasses, which limited the export of nutrients, (ii) the more arid climate prevailing along the southern Tethyan margin (Van de Schootbrugge et al., 2005), and (iii) low dissolved P concentrations in the water column. The slight increase in P_{tot} values recorded during the CIE interval is likely linked to the low sediment-accumulation rate.

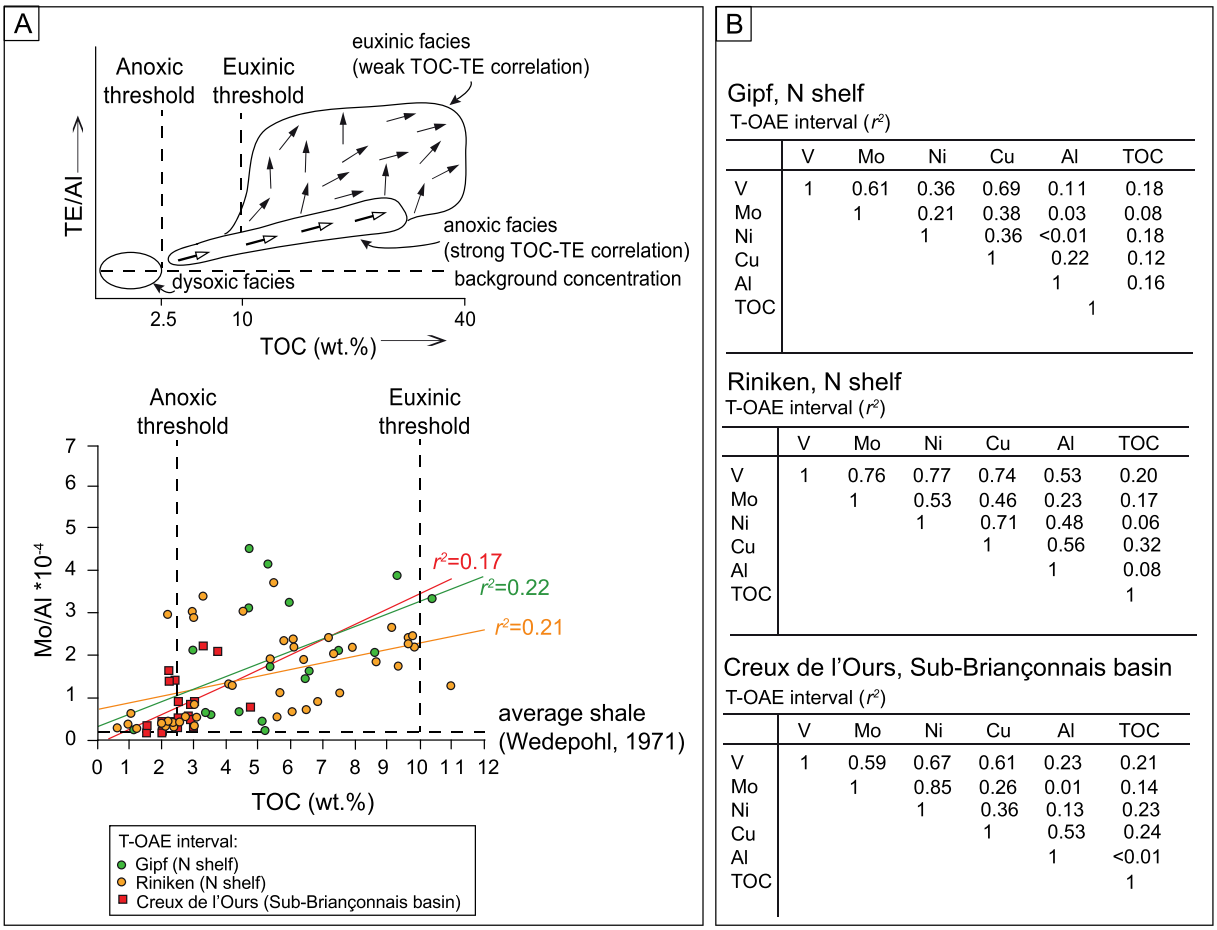

Gipf, N shelf	V	Mo	Ni	Cu	Al	TOC
V	1	0.61	0.36	0.69	0.11	0.18
Mo		1	0.21	0.38	0.03	0.08
Ni			1	0.36	<0.01	0.18
Cu				1	0.22	0.12
Al					1	0.16
TOC						1

Riniken, N shelf	V	Mo	Ni	Cu	Al	TOC
V	1	0.76	0.77	0.74	0.53	0.20
Mo		1	0.53	0.46	0.23	0.17
Ni			1	0.71	0.48	0.06
Cu				1	0.56	0.32
Al					1	0.08
TOC						1

Creux de l'Ours, Sub-Briançonnais basin	V	Mo	Ni	Cu	Al	TOC
V	1	0.59	0.67	0.61	0.23	0.21
Mo		1	0.85	0.26	0.01	0.14
Ni			1	0.36	0.13	0.23
Cu				1	0.53	0.24
Al					1	<0.01
TOC						1

Fig. 11. (A) Comparative Mo-TOC scatterplots for the T-OAE interval from Gipf, Riniken and Creux de l'Ours, according to Algeo and Maynard (2004). Square linear regressions are shown for the three sections. (B) Correlation factors (r^2) of selected trace elements measured in the T-OAE interval at Gipf, Riniken and Creux de l'Ours.

5.5. Depositional conditions during the T-OAE across the Alpine Tethys

The mineralogical and geochemical results from the studied sections bring further insights into the T-OAE, with a particular focus on the environmental and depositional conditions. At Gipf, Riniken (northern shelf) and Creux de l'Ours (Sub-Briançonnais basin), the T-OAE interval is marked by a shift towards warmer and more humid conditions associated with an enhanced hydrological cycle and an increase in continental weathering, as it also occurred elsewhere in the central and NW European basins (Cohen et al., 2004; Brazier et al., 2015; Montero-Serrano et al., 2015; Percival et al., 2016). These conditions coupled with the Early Toarcian transgression promoted nutrient input, and this probably also by the reworking of soils and sediments from the continent into the more proximal basins. Therefore, the paleogeographic position of the sites and their distance away from large landmasses played a role in the distribution of continental input, with the northern shelf (i.e., Gipf and Riniken) likely being more sensitive than the Sub-Briançonnais basin (i.e., Creux de l'Ours). The increase in nutrient availability boosted primary productivity at these sites, which favoured the development of oxygen depleted conditions. Reducing conditions developed as a function of the paleogeography and were enhanced by the thermohaline stratification of the water column, as proposed for European basins (Bjerrum et al., 2001; Van de Schootbrugge et al., 2005; Mattioli et al., 2008; Dera and Donnadieu, 2012; Fantasia et al., in review). Consequently, the development of oxygen depleted conditions promoted benthic regeneration of organic-bound P and its transfer back into the water column (high $C_{org.}/P_{org.}$ ratios), ultimately sustaining primary productivity in a positive feedback loop.

At Breggia, the large distance away from landmasses and/or the presence of a more arid climate likely limited the nutrient input by fluvial discharge. Under such conditions, high primary productivity was not favoured and the oxygen-minimum zone likely not expanded into the Lombardian basin, as was previously suggested (Farrimond et al., 1989). The circulation pattern and the morphology of the Lombardian basin controlled the development of oxygen-depleted conditions, which were restricted to the deepest parts of the basin (Farrimond et al., 1989). This supports previous interpretations that nutrient concentrations were different between the northern and southern Tethyan margin (e.g., Farrimond et al., 1989; Van de Schootbrugge et al., 2005; Reolid et al., 2014).

The studied transect provide further evidence that the onset of the Karoo-Ferrar LIP triggered the profound environmental perturbations associated with the T-OAE and that local conditions modulated the response to this global event (e.g., Cohen et al., 2004; McElwain et al., 2005; McArthur et al., 2008; Hermoso et al., 2009). It is currently thought that the termination of the T-OAE was related to the drawdown of excessive atmospheric CO_2 through enhanced continental weathering and increased organic-carbon burial in the marine realm, thus diminishing the greenhouse effects (Jenkyns, 2003). However, this may be questioned since several sections recording the T-OAE CIE lack significant OM content (e.g., Wignall et al., 2005; McArthur et al., 2008). In addition, most European sections, where high organic-carbon contents are recorded, show relatively low average organic-carbon burial rates (Suan et al., 2016), when compared to modern high-productivity sites (Föllmi et al., 2005). In analogy to Suan et al. (2016), organic-carbon burial rates were calculated for the T-OAE interval at Riniken

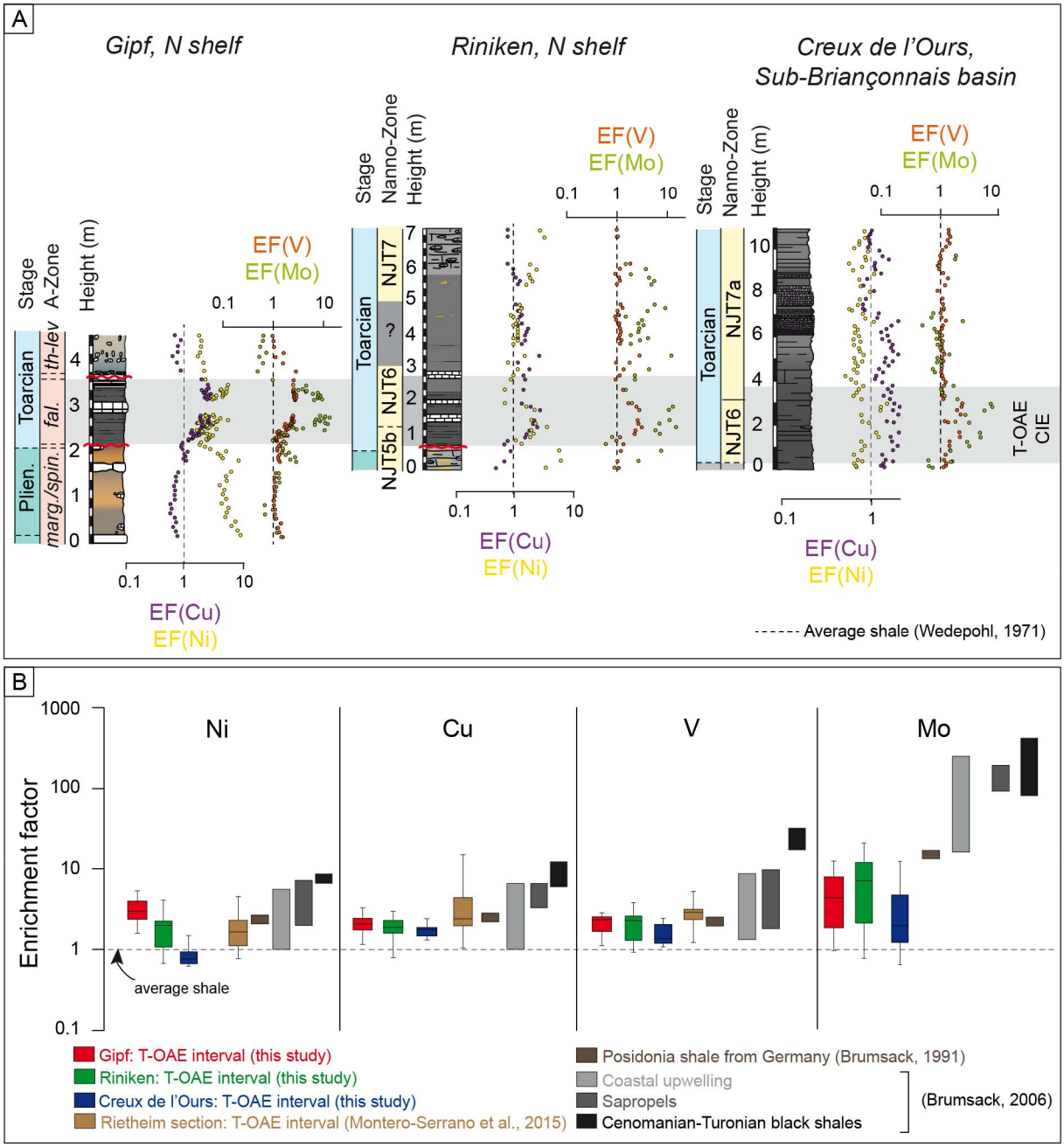

Fig. 12. (A) Evolution of the enrichment factors (EFs) for trace elements (Ni, Cu, V, Mo) measured at Gipf, Riniken and Creux de l'Ours, relative to average shale (Wedepohl, 1971). (B) Enrichment factors (EFs) for Ni, Cu, V and Mo from the T-OAE interval of the studied sections of Gipf, Riniken and Creux de l'Ours compared with other organic-rich sections (Brumsack, 1991, 2006; Montero-Serrano et al., 2015).

and Creux de l'Ours, using average TOC contents (Riniken: 5.9 wt%, Creux de l'Ours: 4.5 wt%), an average density for marly sediments of 1.7 g/cm^3, and a duration for the core of the negative CIE of 450 kyrs (Suan et al., 2008; Ruebsam et al., 2014) or 200 kyrs (Boulila et al., 2014). Calculated organic-carbon burial rates are relatively low (Riniken: 0.24 and 0.55 g/m^2/yr, Creux de l'Ours: 0.57 and 1.29 g/m^2/yr) relative to modern high-productivity sites (e.g., Föllmi et al., 2005), questioning the role of such sites as important sinks for atmospheric CO_2, similar to what was observed for the early Aptian OAE1a (Föllmi, 2012). The development of vegetation in European areas owing to more humid conditions (up to the *bifrons* Zone, Dera et al., 2009) may also have acted as a carbon sink (Westermann et al., 2010; Föllmi, 2012). Recently, it was proposed that the increase in humid conditions favoured the development of large organic-rich lake systems, which significantly contributed to the reduction of the pCO_2 (Xu et al., 2017). The enhancement of fire activity during the T-OAE, and in particular during its termination, may have played an important role in terminating ocean anoxia (Baker et al., 2017).

6. Conclusions

The high-resolution study of five sections recording the CIE provides critical mineralogical and geochemical data, which permit to compare the paleoenvironmental and depositional conditions across the Alpine Tethys during the T-OAE. This transect highlights the different response to the T-OAE depending on the paleogeographic position of the sections, emphasising the importance of local conditions in modulating the impact of the T-OAE. The mineralogical proxies show that the warm

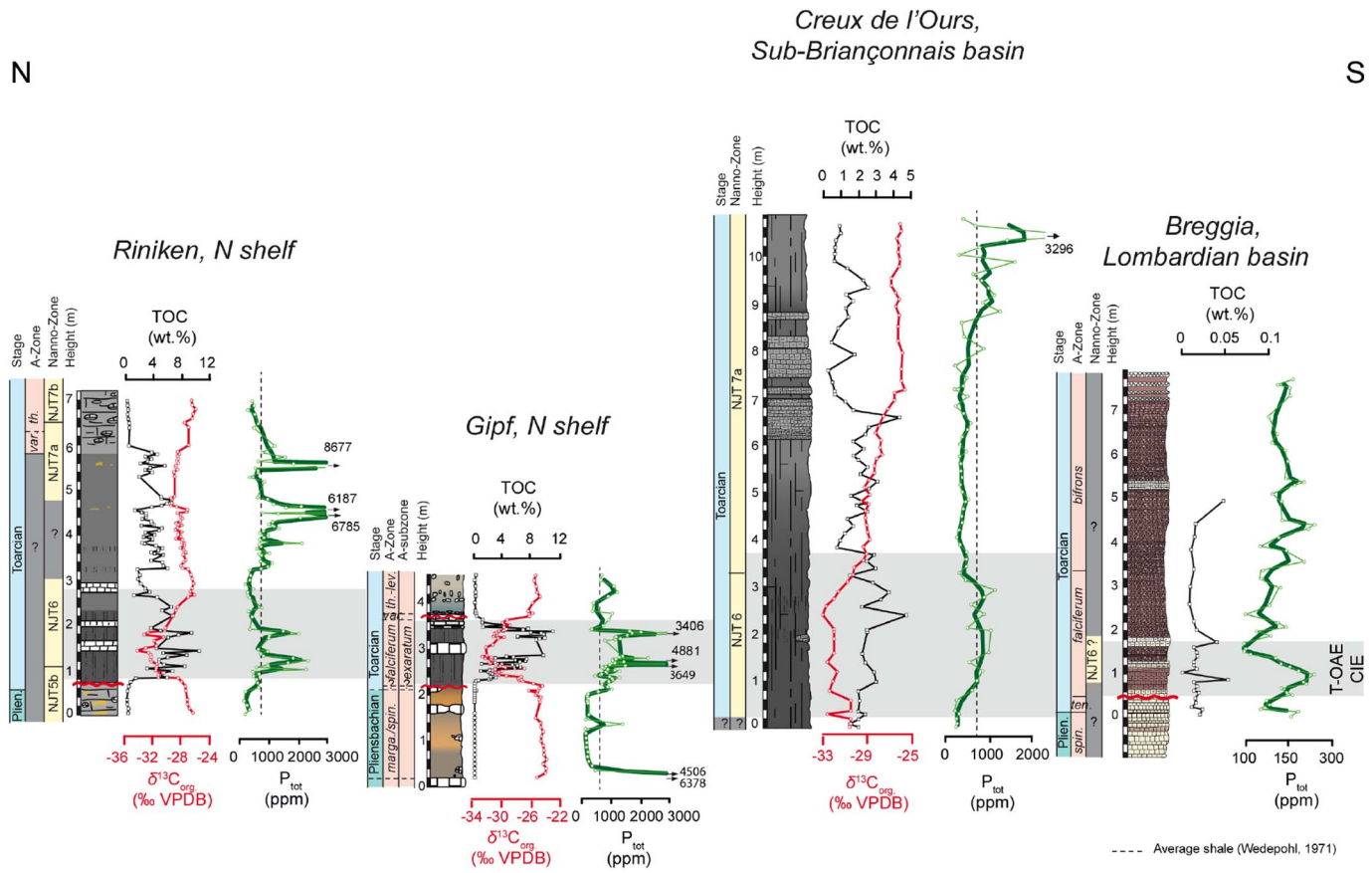

Fig. 13. Variations in phosphorus (P) contents along the studied transect, plotted against the organic-carbon isotopes ($\delta^{13}C_{org}$) and the total organic-carbon (TOC) content.

and humid climate prevailing during the T-OAE led to increased runoff and higher terrigenous input on the northern shelf and in the Sub-Briançonnais basin. The nutrient distribution was probably governed by the proximity to continental masses and likely favoured productivity-driven anoxia in the proximal and more restricted settings. The redox-sensitive TEs show a gradient across the studied transect. Gipf and Riniken (northern shelf) were characterised by dysoxic to anoxic conditions, whereas less reducing conditions were present at Creux de l'Ours (Sub-Briançonnais) and oxic conditions at Breggia (Lombardian basin). Thermohaline stratification promoted reducing conditions and the preservation of the organic matter on the northern shelf and in the Sub-Briançonnais basin. Under such conditions, the release of phosphorus from the sediments into the water column likely sustained the primary productivity, acting as a positive feedback loop. At Breggia, the remote position away from large landmasses and/or the prevalence of low hydrolysing conditions on the continents adjacent to the southern Tethys precluded high nutrient input rates and the resulting primary productivity was low.

Acknowledgements

This research is supported by the Swiss National Science Foundation (project 200021-1495461/1) and the GeoNova project. We acknowledge the NAGRA and the Cantonal Museum of Natural History (Lugano) for their permission to collect samples from the Riniken core and Breggia section, respectively. We would like to thank Jean-Claude Lavanchy and Tiffany Monnier (Institut des Sciences de la Terre, UNIL) for the XRF analyses and help in the laboratory. We acknowledge Matías Reolid and one anonymous reviewer for their constructive review.

References

Abed, A.M., Sadaqah, R.M., 2013. Enrichment of uranium in the uppermost Al-Hisa Phosphorite formation, Eshidiyya basin, southern Jordan. J. Afr. Earth Sci. 77, 31–40.
Adatte, T., Stinnesbeck, W., Keller, G., 1996. Lithostratigraphic and mineralogic correlations of near K/T boundary clastic sediments in northeastern Mexico: implications for origin and nature of deposition. Geol. Soc. Am. Spec. Pap. 307, 211–226.
Adatte, T., Keller, G., Stinnesbeck, W., 2002. Late Cretaceous to early Paleocene climate and sea-level fluctuations: the Tunisian record. Palaeogeogr. Palaeoclimatol. Palaeoecol. 178, 165–196.
Algeo, T., Ingall, E., 2007. Sedimentary C_{org}:P ratios, paleocean ventillation and Phanerozoic atmospheric pO_2. Palaeogeogr. Palaeoclimatol. Palaeoecol. 256, 130–155.
Algeo, T.J., Maynard, J.B., 2004. Trace-element behavior and redox facies in core shales of Upper Pennsylvanian Kansas-type cyclothems. Chem. Geol. 206, 289–318.
Algeo, T.J., Tribovillard, N., 2009. Environmental analysis of paleoceanographic systems based on molybdenum-uranium covariation. Chem. Geol. 211–225.
Al-Suwaidi, A.H., Hesselbo, S.P., Damborenea, S.E., Manceñido, M.O., Jenkyns, H.C., Riccardi, A.C., Angelozzi, G.N., Baudin, F., 2016. The Toarcian oceanic anoxic event (early Jurassic) in the Neuquén Basin, Argentina: a reassessment of age and carbon isotope stratigraphy. J. Geol. 124.
Anderson, L.D., Delaney, M.L., Faul, K.L., 2001. Carbon to phosphorus ratios in sediments: implications for nutrient cycling. Glob. Biogeochem. Cycles 15 (1), 65–79.
Baker, S.J., Hesselbo, S.P., Lenton, T.M., Duarte, L.V., Belcher, C.M., 2017. Charcoal evidence that rising atmospheric oxygen terminated Early Jurassic ocean anoxia. Nat. Commun. 8, 15018.
Baudin, F., Herbin, J.P., Vandenbroucke, M., 1990. Mapping and geochemical characterization of the Toarcian organic matter in the Mediterranean Tethys and Middle East. Org. Geochem. 16, 677–687.
Bernoulli, D., Ulmer, P., 2016. Dropstones in Rosso Ammonitico-facies pelagic sediments of the Southern Alps (southern Switzerland and northern Italy). Swiss J. Geosci. 109, 57–67.
Bjerrum, C.J., Surlyk, F., Callomon, J.H., Singerland, R.L., 2001. Numerical Paleoceanographic study of the Early Jurassic transcontinental Laurasian Seaway. Paleoceanography 16, 390–404.
Blomeier, D.P.G., Reijmer, J.J.G., 1999. Drowning of a Lower Jurassic carbonate platform: Jbel Bou Dahar, High Atlas, Morocco. Facies 41, 81–110.
Bodin, S., Krencker, F.N., Kothe, T., Hoffmann, R., Mattioli, E., Heimhofer, U., Kabiri, L., 2016. Perturbation of the carbon cycle during the late Pliensbachian-early Toarcian: new insight from high-resolution carbon isotope records in Morocco. J. Afr. Earth Sci. 116, 89–104.

Bond, D.P.G., Wignall, P.B., 2014. Large igneous provinces and mass extinctions: an update. In: Keller, G., Kerr, A.C. (Eds.), Impacts and Mass Extinction: Causes and Effects. Spec. Pap., Geol. Soc. Am. 505. pp. 29–55.
Bougeault, C., Pellenard, P., Deconinck, J.-F., Hesselbo, S.P., Dommergues, J.-L., Bruneau, L., Cocquerez, T., Laffont, R., Huret, E., Thibault, N., 2017. Climatic and palaeoceanographic changes during the Pliensbachian (Early Jurassic) inferred from clay mineralogy and stable isotope (C-O) geochemistry (NW Europe). Glob. Planet. Chang. 149, 139–152.
Boulila, S., Galbrun, B., Huret, E., Hinnov, L.A., Rouget, I., Gardin, S., Bartolini, A., 2014. Astronomical calibration of the Toarcian stage: implications for sequence stratigraphy and duration of the early Toarcian OAE. Earth Planet. Sci. Lett. 386, 98–111.
Brazier, J.-M., Suan, G., Tacail, T., Simon, L., Martin, J.E., Mattioli, E., Balter, V., 2015. Calcium isotope evidence for dramatic increase of continental weathering during the Toarcian oceanic anoxic event (Early Jurassic). Earth Planet. Sci. Lett. 411, 164–176.
Brumsack, H.-J., 1991. Inorganic geochemistry of the German Posidonia Shale: paleoenvironmental consequences. In: Tyson, R.V., Pearson, T.H. (Eds.), Modern and Ancient Continental Shelf Anoxia. Geological Society, London, Special Publications 58. pp. 353–362.
Brumsack, H.J., 2006. The trace metal content of recent organic carbon-rich sediments: implications for Cretaceous black shale formation. Palaeogeogr. Palaeoclimatol. Palaeoecol. 232, 344–361.
Burgess, S.D., Bowring, S.A., Fleming, T.H., Elliot, D.H., 2015. High-precision geochronology links the Ferrar large igneous province with early-Jurassic ocean anoxia and biotic crisis. Earth Planet. Sci. Lett. 415, 90–99.
Burtner, R.L., Warner, M.A., 1986. Relationship between illite/smectite diagenesis and hydrocarbon generation in Lower Cretaceous Mowry and Skull Creek Shales of the northern Rocky Mountain area. Clay Clay Miner. 34, 390–402.
Calvert, S.E., Pedersen, T.F., 2007. Elemental proxies for palaeoclimatic and palaeoceanographic variability in marine sediments: interpretation and application. In: Hillaire-Marcel, C., Vernal, A.D. (Eds.), Proxies in Late Cenozoic Paleoceanography. Elsevier, Amsterdam, pp. 567–644.
Caruthers, A.H., Gröcke, D.R., Smith, P.L., 2011. The significance of an Early Jurassic (Toarcian) carbon-isotope excursion in Haida Gwaii (Queen Charlotte Islands), British Columbia, Canada. Earth Planet. Sci. Lett. 307, 19–26.
Chamley, H., 1989. Clay Sedimentology. Springer Verlag, Berlin.
Cohen, A.S., Coe, A.L., Harding, S.M., Schwark, L., 2004. Osmium isotope evidence for the regulation of atmospheric CO_2 by continental weathering. Geology 32, 157–160.
Deconinck, J.-F., Bernoulli, D., 1991. Clay mineral assemblages of Mesozoic pelagic and flysch sediments of the Lombardian Basin (Southern Alps): implications for palaeotectonics, palaeoclimate and diagenesis. Geol. Rundsch. 80, 1–17.
Dera, G., Donnadieu, Y., 2012. Modeling evidences for global warming, Arctic seawater freshening, and sluggish oceanic circulation during the Early Toarcian anoxic event. Paleoceanography 27, PA2211.
Dera, G., Pellenard, P., Neige, P., Deconinck, J.-F., Pucéat, E., Dommergues, J.-L., 2009. Distribution of clay minerals in Early Jurassic Peritethyan seas: palaeoclimatic significance inferred from multiproxy comparisons. Palaeogeogr. Palaeoclimatol. Palaeoecol. 271, 39–51.
Duchamp-Alphonse, S., Fiet, N., Adatte, T., Pagel, M., 2011. Climate and sea-level variations along the northwestern Tethyan margin during the Valanginian C-isotope excursion: mineralogical evidence from the Vocontian Basin (SE France). Palaeogeogr. Palaeoclimatol. Palaeoecol. 302, 243–254.
Eaton, A.D., Clesceri, L.S., Greenberg, A.E., 1995. Standard Methods for the Examination of Water and Waste Water. vol. IXI. pp. 4.113–4.114.
Fantasia, A., Föllmi, K.B., Adatte, T., Spangenberg, J.E., Mattioli, E., (in review). Expression of the Early Toarcian Oceanic Anoxic Event: New Insights from a Swiss Transect.
Farrimond, P., Eglinton, G., Brassell, S.C., Jenkyns, H.C., 1989. Toarcian anoxic event in Europe: an organic geochemical study. Mar. Pet. Geol. 6, 136–147.
Fedo, C., Nesbitt, H.W., Young, G.M., 1995. Unravelling the effects of potassium metasomatism in sedimentary rocks and paleosols, with implications for paleoweathering conditions and provenance. Geology 23, 921–924.
Ferreira, J., Mattioli, E., Pittet, B., Cachão, M., Spangenberg, J.E., 2017. Palaeoecological insights on Toarcian and lower Aalenian calcareous nannofossils from the Lusitanian Basin (Portugal). Palaeogeogr. Palaeoclimatol. Palaeoecol. 436, 245–262.
Filippelli, G.M., Delaney, M.L., 1996. Phosphorus geochemistry of equatorial Pacific sediments. Geochim. Cosmochim. Acta 60, 1479–1495.
Föllmi, K.B., 1995. 160 m.y. record of marine sedimentary phosphorus burial: coupling of climate and continental weathering under greenhouse and icehouse conditions. Geology 23, 859–862.
Föllmi, K.B., 1996. The phosphorus cycle, phosphogenesis and marine phosphate-rich deposits. Earth-Sci. Rev. 40, 55–124.
Föllmi, K.B., 2012. Early Cretaceous life, climate and anoxia. Cretac. Res. 35, 230–257 (Review paper).
Föllmi, K.B., de Kaenel, E., Stille, P., John, C.M., Adatte, T., Steinmann, P., 2005. Phosphogenesis and organic-carbon preservation in the Miocene Monterey Formation at Naples Beach, California-the Monterey hypothesis revisited. GSA Bull. 117, 589–619.
Fu, X., Wang, J., Zeng, S., Feng, X., Wang, D., Song, C., 2017. Continental weathering and paleoclimatic changes through the onset of the Early Toarcian oceanic anoxic event in Qiangtang Basin, eastern Tethys. Palaeogeogr. Palaeoclimatol. Palaeoecol. 302 (487), 241–250.
Gibbs, R.J., 1977. Clay-mineral segregation in the marine environment. J. Sediment. Petrol. 47, 237–243.
Godet, A., Bodin, S., Adatte, T., Föllmi, K.B., 2008. Platform-induced clay-mineral fractionation along a northern Tethyan basin-platformtransect: implications for the interpretation of Early Cretaceous climate change (Late Hauterivian–Early Aptian). Cretac. Res. 29, 830–847.
Gröcke, D.R., Hori, R.S., Trabucho-Alexandre, J., Kemp, D.B., Schwark, L., 2011. An open ocean record of the Toarcian oceanic anoxic event. Solid Earth 2, 245–257.
Haq, B.U., 2017. Jurassic sea-level variations: a reappraisal. Geol. Soc. Am. 18 (1).
Haq, B.U., Hardenbol, J., Vail, P.R., 1987. Chronology of fluctuating sea levels since the Triassic. Science 235, 1156–1167.
Hardenbol, J., Thierry, J., Farley, M.B., de Graciansky, P.-C., Vail, P.R., 1998. Mesozoic and Cenozoic sequence chronostratigraphic framework of European basins. In: de Graciansky, P.-C., Hardenbol, J., Jacquin, T., Vail, P.R. (Eds.), Mesozoic and Cenozoic Sequence Stratigraphy of European Basins. SEPM Spec. Publ. 60. pp. 3–13.
Harries, P.J., Little, C.T.S., 1999. The early Toarcian (Early Jurassic) and the Cenomanian–Turonian (Late Cretaceous) mass extinctions: similarities and contrasts. Palaeogeogr. Palaeoclimatol. Palaeoecol. 154, 39–66.
Hermoso, M., Pellenard, P., 2014. Continental weathering and climatic changes inferred from clay mineralogy and paired carbon isotopes across the early to middle Toarcian in the Paris Basin. Palaeogeogr. Palaeoclimatol. Palaeoecol. 399, 385–393.
Hermoso, M., Minoletti, F., Le Callonnec, L., Jenkyns, H.C., Hesselbo, S.P., Rickaby, R.E.M., Renard, M., de Rafélis, M., Emmanuel, L., 2009. Global and local forcing of Early Toarcian seawater chemistry: a comparative study of different paleoceanographic settings (Paris and Lusitanian basins). Paleoceanography 24, 1–15.
Hermoso, M., Minoletti, F., Rickaby, R.E.M., Hesselbo, S.P., Baudin, F., Jenkyns, H.C., 2012. Dynamics of a stepped carbon-isotope excursion: ultra high-resolution study of Early Toarcian environmental change. Earth Planet. Sci. Lett. 319-320, 45–54.
Hesselbo, S.P., Jenkyns, H.C., Duarte, L.V., Oliveira, L.C.V., 2007. Carbon-isotope record of the Early Jurassic (Toarcian) oceanic anoxic event from fossil wood and marine carbonate (Lusitanian Basin, Portugal). Earth Planet. Sci. Lett. 253, 455–470.
Jenkyns, H.C., 1988. The early Toarcian (Jurassic) anoxic event; stratigraphic, sedimentary and geochemical evidence. Am. J. Sci. 288, 101–151.
Jenkyns, H.C., 2003. Evidence for rapid climate change in the Mesozoic–Palaeogene greenhouse world. Philos. Trans. R. Soc. London, Ser. A 361, 1885–1916.
Jenkyns, H.C., 2010. Geochemistry of oceanic anoxic events. Geochem. Geophys. Geosyst. 11.
Jenkyns, H.C., Gröcke, D.R., Hesselbo, S.P., 2001. Nitrogen isotope evidence for water mass denitrification during the early Toarcian (Jurassic) oceanic anoxic event. Paleoceanography 16, 593–603.
Kemp, D.B., Izumi, K., 2014. Multiproxy geochemical analysis of a Panthalassic margin record of the early Toarcian oceanic anoxic event (Toyora area, Japan). Palaeogeogr. Palaeoclimatol. Palaeoecol. 414, 332–341.
Kemp, D.B., Coe, A.L., Cohen, A.S., Weedon, G.P., 2011. Astronomical forcing and chronology of the early Toarcian (Early Jurassic) oceanic anoxic event in Yorkshire, UK. Paleoceanography 26.
Klug, H.P., Alexander, L., 1974. X-ray Diffraction Procedures for Polycrystalline and Amorphous Materials, First and Second editions. John Wiley and Sons, Inc., New York.
Kübler, B., 1983. Cristallinité de l'illite, méthodes normalisées de préparations, méthodes normalisées de mesures. série ADX Cahiers Institut Géologie de Neuchâtel, Suisse.
Kübler, B., 1987. Cristallinité de l'illite : méthode normalisée de préparation de mesure, méthode automatique normalisée de mesure. Séries AX, 3.1 and 3.2 1–3 Cahiers de l'Institut de Géologie.
Kübler, B., Jaboyedoff, M., 2000. Illite crystallinity. Comptes Rendus de l'Académie des Sciences Paris Sciences de la Terre et des planètes série ADX 1, 1–13. Earth Planet. Sci. 331, 75–89.
Kuhn, O., Etter, W., 1994. Der Posidonienschiefer der Nordschweiz: Lithostratigraphie, Biostratigraphie, Fazies. Eclogae Geol. Helv. 87 (1), 113–138.
Matter, A., Peters, T., Isenschmid, C., Bläsi, H.R., Ziegler, H.-J., 1987. Sondierbohrung Riniken – Geologie. Nagra Tech. Ber., 86-02, Nagra, Wettingen.
Mattioli, E., Pittet, B., Suan, G., Mailliot, S., 2008. Calcareous nannoplankton changes across the early Toarcian oceanic anoxic event in the western Tethys. Paleoceanograhy 23.
Mattioli, E., Pittet, B., Petitpierre, L., Mailliot, S., 2009. Dramatic decrease of pelagic carbonate production by nannoplankton across the Early Toarcian anoxic event (T-OAE). Glob. Planet. Chang. 65 (3–4), 134–145.
McArthur, J.M., Algeo, T.J., van de Schootbrugge, B., Li, Q., Howarth, R.J., 2008. Basinal restrictions, black shales, Re-Os dating, and the early Toarcian (Jurassic) oceanic anoxic event. Paleoceanography 23 (4).
McElwain, J.C., Wade-Murphy, J., Hesselbo, S.P., 2005. Changes in carbon dioxide during an oceanic anoxic event linked to intrusion into Gondwana coals. Nature 435, 479–482.
McLennan, S.M., Hemming, S., McDaniel, D.K., Hanson, G.N., 1993. Geochemical approaches to sedimentation, provenance and tectonics. Geol. Soc. Am. Spec. Pap. 284.
Mettraux, M., Mosar, J., 1989. Tectonique alpine et paléotectonique liasique dans les Préalpes Médianes en rive droite du Rhône. Eclogae Geol. Helv. 82, 517–540.
Montero-Serrano, J.-C., Föllmi, K.B., Adatte, T., Spangenberg, J.E., Tribovillard, N., Fantasia, A., Suan, G., 2015. Continental weathering and redox conditions during the early Toarcian oceanic anoxic event in the northwestern Tethys: insight from the Posidonia Shale section in the Swiss Jura Mountains. Palaeogeogr. Palaeoclimatol. Palaeoecol. 429, 83–99.
Mort, H., Adatte, T., Föllmi, K.B., Keller, G., Steinmann, P., Matera, V., Berner, Z., Stüben, D., 2007. Phosphorus and the roles of productivity and nutrient recycling during Oceanic Anoxic Event 2. Geology 35 (6), 483–486.
Nesbitt, H.W., Young, G.M., 1989. Formation and diagenesis of weathering profiles. J. Geol. 97 (2), 129–147.
Nordstrom, D.K., 1982. Aqueous pyrite oxidation and the consequent formation of secondary iron minerals. In: Kittrick, J.A., Fanning, D.F., Hossner, L.R. (Eds.), Acid Sulfate Weathering: Pedogeochemistry and Relationship to Manipulation of Soil Materials. Soil Science Society of Americapp. 37–56.

Pálfy, J., Smith, P.L., 2000. Synchrony between Early Jurassic extinction, oceanic anoxic event, and the Karoo-Ferrar flood basalt volcanism. Geology 28, 747–750.
Percival, L.M.E., Cohen, A.S., Davies, M.K., Dickson, A.J., Hesselbo, S.P., Jenkyns, H.C., Leng, M.J., Mather, T.A., Storm, M.S., Xu, W., 2016. Osmium isotope evidence for two pulses of increased continental weathering linked to Early Jurassic volcanism and climate change. Geology 44, 759–762.
Redfield, A.C., 1958. The biological control of chemical factors in the environment. Am. Sci. 46, 205–222.
Reolid, M., 2014. Stable isotopes on foraminifera and ostracods for interpreting incidence of the Toarcian oceanic anoxic event in Westernmost Tethys: role of water stagnation and productivity. Palaeogeogr. Palaeoclimatol. Palaeoecol. 395, 77–91.
Reolid, M., Mattioli, E., Nieto, L.M., Rodríguez-Tovar, F., 2014. The Early Toarcian oceanic anoxic event in the external Subbetic (Southiberian Palaeomargin, Westernmost Tethys): geochemistry, nannofossils and ichnology. Palaeogeogr. Palaeoclimatol. Palaeoecol. 411, 79–94.
Rieber, H., 1973. Fauna und Stratigraphie einer oolithischen Kalkbank aus dem Toarcium von Gipf (Kanton Aargau, Schweiz). Eclogae Geol. Helv. 66 (3), 657–665.
Riquier, L., Tribovillard, N., Averbuch, O., Devleeschouwer, X., Riboulleau, A., 2006. The Late Frasnian Kellwasser horizons of the Harz Mountains (Germany): two oxygen deficient periods resulting from different mechanisms. Chem. Geol. 233, 137–155.
Röhl, H.J., Schmid-Röhl, A., Oschmann, W., Frimmel, A., Schwark, L., 2001. The Posidonia Shale (Lower Toarcian) of SW-Germany: an oxygen-depleted ecosystem controlled by sea level and palaeoclimate. Palaeogeogr. Palaeoclimatol. Palaeoecol. 165, 27–52.
Ruebsam, W., Münzberger, P., Schwark, L., 2014. Chronology of the Early Toarcian environmental crisis in the Lorraine Sub-Basin (NE Paris Basin). Earth Planet. Sci. Lett. 404, 273–282.
Ruttenberg, K.C., 1992. Development of a sequential extraction method for different forms of phosphorus in marine sediments. Limnol. Oceanogr. 37, 1460–1482.
Schenau, S.J., de Lange, G.J., 2000. A novel chemical method to quantify fish debris in marine sediments. Limnol. Oceanogr. 45, 963–971.
Singer, A., 1984. The palaeoclimatic interpretation of clay minerals in sediments – a review. Earth Sci. Rev. 21, 251–293.
Slomp, C.P., Epping, E.H.G., Helder, W., Van Raaphorst, W., 1996. A key for iron-bound phosphorus in authigenic apatite formation in North Atlantic continental platform sediments. J. Mar. Res. 54, 1179–1205.
Suan, G., Pittet, B., Bour, I., Mattioli, E., Duarte, L.V., Mailliot, S., 2008. Duration of the Early Toarcian carbon isotope excursion deduced rom spectral analysis: consequence for its possible causes. Earth Planet. Sci. Lett. 267, 666–679.
Suan, G., Nikitenko, B.L., Rogov, M.A., Baudin, F., Spangenberg, J.E., Knyazev, V.G., Glinskikh, L.A., Goryacheva, A.A., Adatte, T., Riding, J.B., Föllmi, K.B., Pittet, B., Mattioli, E., Lécuyer, C., 2011. Polar record of early Jurassic massive car-bon injection. Earth Planet. Sci. Lett. 312, 102–113.
Suan, G., van de Schootbrugge, B., Adatte, T., Fiebig, J., Oschmann, W., 2015. Calibrating the magnitude of the Toarcian carbon cycle perturbation. Paleoceanography 30, 495–509.
Suan, G., Schlögl, J., Mattioli, E., 2016. Bio-and chemostratigraphy of the Toarcian organic-rich deposits of some key successions of the Alpine Tethys. Newsl. Stratigr. 49 (3), 401–419.
Svensen, H., Planke, S., Chevallier, L., Malthe-Sørenssen, A., Corfu, F., Jamtveit, B., 2007. Hydrothermal venting of greenhouse gases triggering Early Jurassic global warming. Earth Planet. Sci. Lett. 256, 554–566.
Them II, T.R., Gill, B.C., Caruthers, A.H., Gröcke, D.R., Tulsky, E.T., Martindale, R.C., Poulton, T.P., Smith, P.L., 2017. High-resolution carbon isotope records of the Toarcian oceanic anoxic event (Early Jurassic) from North America and implications for the global drivers of the Toarcian carbon cycle. Earth Planet. Sci. Lett. 459, 118–126.
Thierry, J., 2000. Late Toarcian. In: Dercourt, J., Gaetani, M., Vrielynck, B., Barrier, E., Biju-Duval, B., Brunet, M.F., Cadet, J.P., Crasquin, S., Sandulescu, M. (Eds.), Atlas Peri-Tethys. Palaeogeographical Maps.
Thiry, M., 2000. Palaeoclimatic interpretation of clay minerals in marine deposits: an outlook from the continental origin. Earth-Sci. Rev. 49, 201–221.
Todorov, I., Schegg, R., Wildi, W., 1993. Thermal maturity and modelling of Mesozoic and Cenozoic sediments in the south of the Rhine Graben and the Eastern Jura (Switzerland). Eclogae Geol. Helv. 86 (3), 667–692.
Trecalli, A., Spangenberg, J.E., Adatte, T., Föllmi, K.B., Parente, M., 2012. Carbonate platform evidence of ocean acidification at the onset of the early Toarcian oceanic anoxic event. Earth Planet. Sci. Lett. 357–358, 214–225.
Tribovillard, N., Algeo, T.J., Lyons, T., Riboulleau, A., 2006. Trace metals as paleoredox and paleoproductivity proxies: an update. Chem. Geol. 232 (1–2), 12–32.
Tröster, J., 1987. Biostratigraphie des Obertoarcium und der Toarcium/Aalenium-Grenze der Bohrungen Weiach, Beznau, Riniken und Schafisheim (Nordschweiz). Eclogae Geol. Helv. 80, 431–447.
Tyrell, T., 1999. The relative influences of nitrogen and phosphorus on oceanic primary production. Nature 400, 525–531.
Van Cappellen, P., Ingall, E.D., 1994. Benthic phosphorus regeneration, net primary production, and ocean anoxia: a model of the coupled marine biogeochemical cycles of carbon and phosphorus. Paleoceanography 9, 677–692.
Van de Schootbrugge, B., McArthur, J.M., Bailey, T.R., Rosenthal, J.D., Wright, J.D., Miller, K.G., 2005. Toarcian oceanic anoxic event: an assessment of global causes using belemnite C isotope records. Paleoceanography 29, 1–10.
Velde, B., 1995. Origin and mineralogy of clays. In: Clays and the Environment. Springer Verlag (334 pp.).
Wedepohl, K.H., 1971. Environmental influences on the chemical composition of shales and clays. In: Ahrens, L.H., Press, F., Runcorn, S.K., Urey, H.C. (Eds.), Physics and Chemistry of the Earth. Oxford, Pergamon, pp. 307–331.
Westermann, S., Föllmi, K.B., Adatte, T., Matera, V., Schnyder, J., Fleitmann, D., Fiet, N., Ploch, I., Duchamp-Alphonse, S., 2010. The Valanginian $\delta^{13}C$ excursion may not be an expression of a global oceanic anoxic event. Earth Planet. Sci. Lett. 290, 118–131.
Westermann, S., Duchamp-Alphonse, S., Fiet, N., Fleitmann, D., Matera, V., Adatte, T., Föllmi, K.B., 2013. Paleoenvironmental changes during the Valanginian: new insights from variations in phosphorus contents and bulk-and clay mineralogies in the western Tethys. Palaeogeogr. Palaeoclimatol. Palaeoecol. 392, 196–208.
Wiedenmayer, F., 1980. Die Ammoniten der Mediterranen Provinz im Pliensbachian und unteren Toarcian aufgrund neuer Untersuchungen im Generoso-Becken (Lombardische Alpen). In: Denkschriften der Schweizerischen Naturforschenden Gesellschaft. 93 (263 pp).
Wignall, Maynard, 1993. The sequence stratigraphy of transgressive black shales. In: Katz, B., Pratt, L.M. (Eds.), Source Rocks in a Sequence Stratigraphic Framework AAPG Studies in Geology. vol. 37. pp. 35–47.
Wignall, P.B., Newton, R.J., Little, C.T.S., 2005. The timing of paleoenvironmental change and cause-and-effect relationships during the Early Jurassic mass extinction in Europe. Am. J. Sci. 305, 1014–1032.
Winterer, E.L., Bosellini, A., 1981. Subsidence and sedimentation on Jurassic passive continental margin, Southern Alps, Italy. AAPG Bull. 65, 394–421.
Xu, W., Ruhl, M., Jenkyns, H.C., Hesselbo, S.P., Riding, J.B., Selby, D., Naafs, B.D.A., Weijers, J.W.H., Pancost, R., Tegelaar, E., Idiz, E.F., 2017. Carbon sequestration in an expanded lake system during the Toarcian oceanic anoxic event. Nat. Geosci. 10, 129–135.